Journal of Rock Mechanics and Geotechnical Engineering 14 (2022) 560–575

Contents lists available at ScienceDirect

Journal of Rock Mechanics and Geotechnical Engineering

journal homepage: www.jrmge.cn

Full Length Article

Seismic bearing capacity of a strip footing on rock media

Obaidur Rahaman, Jyant Kumar*

Department of Civil Engineering, Indian Institute of Science, Bangalore, Karnataka, 560012, India

ARTICLE INFO

Article history:
Received 22 March 2021
Received in revised form
28 June 2021
Accepted 19 August 2021
Available online 10 December 2021

Keywords:
Earthquake loads
Limit analysis
Lower bound
Power cone programming (PCP)
Rock mass
Strip footing

ABSTRACT

The bearing capacity factors for a rough strip footing placed on rock media, which is subjected to pseudo-static horizontal earthquake body forces, have been determined using the lower bound finite element limit analysis in conjunction with the power cone programming (PCP). The rock mass is assumed to follow the generalized Hoek-Brown (GHB) yield criterion. No assumption needs to be made to smoothen the GHB yield criterion and the convergence is found to achieve quite rapidly while performing the optimization with the usage of the PCP. While incorporating the variation in horizontal earthquake acceleration coefficient (k_h), the effect of changes in unit weight of rock mass (γ), ground surcharge pressure (q_0) and the associated GHB material shear strength parameters (geological strength index (*GSI*), yield parameter (m_i), uniaxial compressive strength (σ_{ci})) on the bearing capacity factors has been thoroughly assessed. Non-dimensional charts have been developed for design purpose. The accuracy of the present analysis has been duly checked by comparing the obtained results with the different solutions reported in the literature. The failure patterns have also been examined in detail.

1. Introduction

A number of studies have been performed in the literature to determine the bearing capacity for different types of foundations resting over rock media (Serrano and Olalla, 1994, 1996; Serrano et al., 2000; Yang et al., 2003; Yang and Yin, 2005; Saada et al., 2008, 2011; Merifield et al., 2006; Yang, 2009; Keshavarz et al., 2016; Kumar and Mohapatra, 2017; Keshavarz and Kumar, 2021). Using the stress characteristics method, Serrano and Olalla (1994) computed the bearing capacity of a strip footing placed over weightless rock media, with horizontal ground surface, on the basis of the original Hoek-Brown failure criterion (Hoek and Brown, 1980). The same methodology was later employed by Serrano and Olalla (1996) to compute the bearing capacity of a strip footing placed over weightless rock media but with sloping ground surface. Serrano et al. (2000) obtained the bearing capacity of a strip footing over rock media to consider the modified version of the Hoek-Brown failure criterion (Hoek et al., 1992). Using the lower bound (LB) limit analysis but with an assumption of the failure mechanism and using the modified Hoek-Brown criterion, Yang et al. (2003) computed the bearing capacity of a strip footing resting over weightless rock media. The upper bound (UB) solution for computing the bearing capacity based on the generalized Hoek-Brown (GHB) yield criterion (Hoek et al., 2002) was obtained by Yang and Yin (2005), using a generalized tangential technique and with an assumption of the multi-wedge translation failure mechanism. In this method, instead of using the actual GHB failure criterion, a linearized Mohr-Coulomb failure criterion, which remains always tangential to the GHB failure envelope, was used. This procedure was, however, found to overestimate the actual ultimate bearing capacity as demonstrated by Saada et al. (2008). Merifield et al. (2006) employed the lower and UB finite element limit analysis (FELA) technique and bracketed the ultimate bearing capacity of a strip footing on rock masses approximately within 2%. The effects of the inclination of a rock slope, ranging from 0° to 30°, and the horizontal seismic coefficient k_h, ranging from 0 to 0.2, on the bearing capacity factor of a strip footing placed on the edge of a rock slope, have been examined by Yang (2009), using the UB theorem of the limit analysis, based on the methodology proposed by Yang and Yin (2005). Saada et al. (2011) implemented the kinematic approach of the limit analysis to determine the reduction in the bearing capacity of a spread footing placed on rock slopes with an inclusion of the seismic forces. The ultimate bearing capacity of a strip footing placed on weightless rock media in the presence of seismic forces has also been assessed by Keshavarz et al. (2016) using the stress characteristic method and with the usage of the earlier version of the Hoek-Brown yield criterion (Hoek and

* Corresponding author.
E-mail address: jkumar@iisc.ac.in (J. Kumar).
Peer review under responsibility of Institute of Rock and Soil Mechanics, Chinese Academy of Sciences.

https://doi.org/10.1016/j.jrmge.2021.08.017

Brown, 1980). Keshavarz and Kumar (2021) also computed the bearing capacity of a ring foundation using the stress characteristics method and the obtained solution was also compared with that computed on the basis of the FELA.

Amongst the numerous methods for solving different geomechanics stability problems, the FELA (Lysmer, 1970; Sloan, 1988) is the most rigorous one in terms of accuracy and computational efficiency. It inherits a number of advantages over the other conventional stability methods (Sloan, 2013). Unlike the limit equilibrium method, this method does not require any kind of assumption associated with the failure mechanism. Rather, this method generates the actual collapse mechanism from the analysis. Like the displacements based elasto-plastic finite element method, it can handle irregular geometry, complicated boundary condition, complex loading condition, material anisotropy and inhomogeneity. In the elasto-plastic finite element method, the definition of the complete material constitutive relationship is necessary. On the other hand, the FELA considers the problem only on the verge of failure/collapse. Therefore, in the FELA, it requires only the shear strength parameters for performing the stability analysis. Unlike the conventional elasto-plastic finite element method, the need of any step-by-step incremental analysis is completely avoided in the FELA which eventually results in saving of the computational cost.

Over the years, the efficiency of this methodology has been significantly improved especially with an introduction to the conic programming techniques such as the second order cone programming (SOCP) (Makrodimopoulos and Martin, 2006) and the semi-definite programming (SDP) (Krabbenhoft et al., 2008). For the rock mass obeying the Hoek-Brown yield criterion, Kumar and Mohapatra (2017) applied the SDP technique which is computationally more efficient than the nonlinear programming (NLP), to determine the bearing capacity factors for strip and circular footing based on the LB FELA. The same technique was later implemented by Ukritchon and Keawsawasvong (2018) for dealing with various three-dimensional (3D) stability problems. The proposed SDP formulation, however, overestimates the bearing capacity factors as it requires a slight modification in the GHB criterion where the value of the exponential factor needs to be kept equal to 0.5. This limitation was later overcome by Kumar and Rahaman (2020) by implementing the power cone programming (PCP) while employing the LB FELA. This technique was also proved to be computationally more efficient.

Although a number of studies with different methodologies are available to estimate the ultimate bearing capacity of a strip footing under static condition, only a few investigations have been performed to account for the consideration of the seismic forces. Most of the existing studies related to the seismic bearing capacity factors are based on the UB analysis (Yang, 2009; Saada et al., 2011) or the slip line method (Keshavarz et al., 2016); in both the methods a predefined failure mechanism has been assumed. Moreover, these studies do not consider the most recent GHB failure criterion (Hoek and Brown, 2019) in its true form. The present study examines the effect of the pseudo-static earthquake inertial body forces while computing the bearing capacity factors for a strip footing resting over rock media and subjected to surcharge pressure. The current analysis is based on the application of the LB FELA and the PCP. The analysis involves the implementation of the GHB yield criterion in its true form without requiring any kind of assumption associated with the smoothing of the GHB yield criterion.

2. The yield criterion for rock mass

Among the various failure criteria proposed in the literature, the GHB failure criterion as proposed by Hoek et al. (2002) was considered to be the most acceptable basis for modelling the shear strength of rock mass. This yield criterion was developed through a series of laboratory tests which covered numerous types of undisturbed and disturbed rock specimens over a wide range of confining stresses. This criterion is used extensively by practitioners for a variety of rock engineering projects (Ulusay, 2014). By Using this criterion, a number of stability problems have been solved: for instance, (i) the determination of the bearing capacity of footings (Merifield et al., 2006; Chakraborty and Kumar, 2015); (ii) the stability of slopes (Li et al., 2008); and (iii) the stability of tunnels (Suchowerska et al., 2012; Ukritchon and Keawsawasvong, 2019; Rahaman and Kumar, 2020). The latest GHB criterion (Hoek et al., 2002; Hoek and Brown, 2019), which is followed in this study, has been written in the following form:

$$\sigma_1 - \sigma_3 - \left[-m_b\sigma_1(-\sigma_{ci})^{(1-\alpha)/\alpha} + s(-\sigma_{ci})^{1/\alpha} \right]^{\alpha} \leq 0 \tag{1}$$

Note that in the above expression, there is a change in the sign convention as compared to failure criterion reported by Hoek and Brown (2019). In this expression, the tensile normal stress is considered to be positive. The variables σ_1 and σ_3 imply the major and minor principal stresses at failure, respectively; and σ_{ci} defines the uniaxial compressive strength of the rock specimen. The strength parameters m_b, s and α are described by the following equations:

$$m_b = m_i \exp\left(\frac{GSI - 100}{28 - 14D}\right) \tag{2a}$$

$$s = \exp\left(\frac{GSI - 100}{9 - 3D}\right) \tag{2b}$$

$$\alpha = \frac{1}{2} + \frac{1}{6}\left[\exp(-GSI/15) - \exp(-20/3)\right] \tag{2c}$$

Note that all these parameters are a function of the geological strength index (GSI), disturbance factor (D) and the yield parameter (m_i). The parameter GSI signifies a measure of the rock mass strength under different geological conditions. The range of the GSI typically varies from 10 for an extremely poor rock to 100 for an intact rock mass. The factor D is a disturbance coefficient that incorporates the disturbance of the rock mass which may occur for instance due to blast damage, impact loading and sudden stress relaxation. It varies from 0 for an undisturbed rock mass to 1 for very disturbed rock mass. The parameter m_i which can be obtained from triaxial compression test data is analogous to the frictional strength of the intact rock mass. The approximate values of m_i for different types of rocks are described in detail by Hoek (1990). It has an approximate range of 5–35.

3. Description of the problem

A strip footing of width B is placed on rock media with horizontal ground surface, as shown in Fig. 1a. The footing is assumed to be perfectly rough. The rock mass has a unit weight γ and the ground surface is subjected to vertical uniform surcharge pressure of q_0. The rock mass is assumed to follow the GHB yield criterion. This study employs the pseudo-static approach to consider the influence of seismic inertial forces in the system. The rock media and the overlying superstructure are subjected to horizontal seismic acceleration of $k_h g$, where k_h is the acceleration coefficient, and g is the acceleration due to gravity. The load on the footing comes from the superstructure weight and the horizontal pseudo-static earthquake inertial forces. If the vertical load on the footing per unit length at collapse is Q_u, the footing will be subjected to a

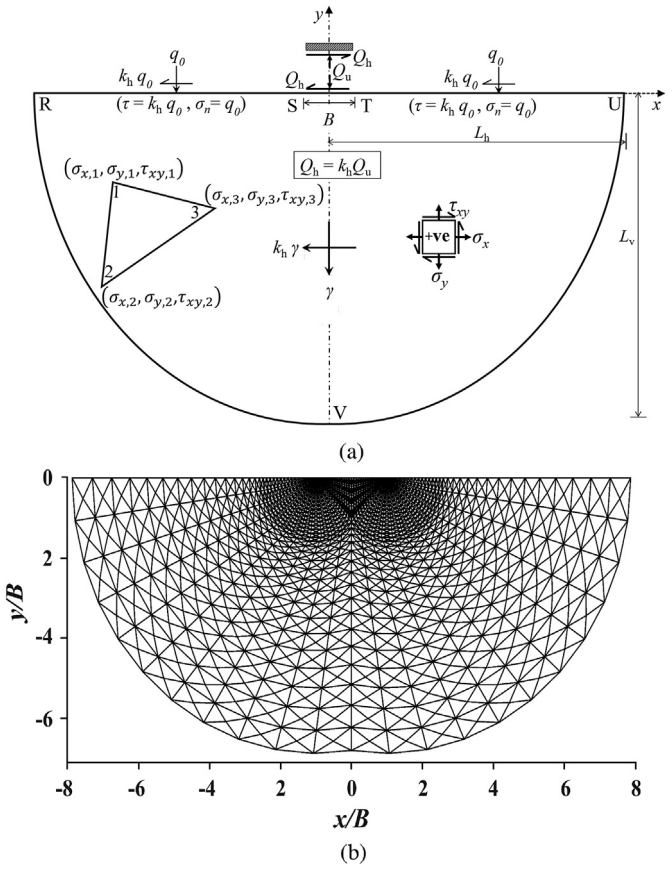

Fig. 1. (a) Problem definition and stress boundary conditions, and (b) A typical chosen mesh.

horizontal shear force of $k_h Q_u$ along the interface of the footing and underlying rock mass. Similarly, if the ground surface is loaded with a surcharge pressure of q_0, it will also be subjected to a uniform shear stress of $k_h q_0$. The rock media will be subjected to body forces per unit volume of γ and $k_h\gamma$ in vertical and horizontal directions, respectively. It is to determine the magnitude of Q_u for various specified values of material parameters defining the GHB yield criterion, and different values of γ, q_0 and k_h.

It should be mentioned that the best way to analyze the stability of any structure due to occurrence of an earthquake is to perform a dynamic analysis with the consideration of the actual/design acceleration-time history. However, this kind of approach often requires a complex numerical analysis which in turn needs quite high computational effort. In most of the geotechnical stability analyses in the presence of seismic forces, the conventional pseudo-static method is often employed to determine the stability of any structure in the event of occurrence of an earthquake. In this approach, the seismic inertial force is replaced by an equivalent static force which is calculated by multiplying the unit weight of the medium with the seismic acceleration coefficient. The magnitude of the seismic acceleration coefficient is determined from the knowledge of the peak ground acceleration (PGA) for the design earthquake. The analysis following the pseudo-static method is generally considered to be conservative (Li et al., 2009; Yang, 2009; Saada et al., 2011). Despite its limitations, the conventional pseudo-static method is widely employed due to its simplicity and ease in implementation. In the presence of seismic forces, this method has been applied by various researchers for finding the solutions of numerous geotechnical stability problems, such as finding (i) the bearing capacity of foundations resting on horizontal ground surface (Kumar and Rao, 2002; Keshavarz et al., 2016), (ii) the bearing capacity of foundation on slopes (Kumar and Rao, 2003; Saada et al., 2011; Kumar and Chakraborty, 2013), and (iii) the stability of slopes (Li et al., 2009), tunnels (Sahoo and Kumar, 2012; Saada et al., 2013), and retaining walls (Kumar 2001; Conte et al., 2017; Chehade et al., 2021). The pseudo-static approach is also used to countercheck the results of a more sophisticated dynamic analysis. Therefore, this approach has been employed in the current research.

4. Analysis

In order to solve the stability problem which involves layers, complicated geometry and complex boundary conditions, the FELA is proved to be a powerful tool. This method involves (i) the LB and UB limit theorems of the plasticity, (ii) the discretization technique of the finite elements, and (iii) an optimization technique. Although both the LB and UB solutions help to bracket the true limit load in a bound form, in practice, however, the LB analysis predicts a collapse load which is always less than or equal to the true answer. In the present study, the LB FELA is employed for the computation of the safe design load.

4.1. Finite elements

The very first step in the formulation of the LB FELA is to discretize the selected domain with a mesh of chosen finite elements. The present study employs the three noded linear stress triangular elements. The chosen problem domain and a typical triangular element with the unknown nodal stresses (σ_x, σ_y and τ_{xy}) are presented in Fig. 1a. The stresses (σ_x, σ_y and τ_{xy}) at any point within the element are assumed to vary linearly according to the following expressions:

$$\sigma_x = \sum_{i=1}^{3} N_i \sigma_{x,i},\ \sigma_y = \sum_{i=1}^{3} N_i \sigma_{y,i},\ \tau_{xy} = \sum_{i=1}^{3} N_i \tau_{xy,i} \tag{3}$$

where $\sigma_{x,i}$, $\sigma_{y,i}$ and $\tau_{xy,i}$ are the stresses at the node i, and the parameter N_i represents the linear shape function. If the coordinate of the node i is denoted by (x_i, y_i) and the three nodes of a triangular element are numbered in a counterclockwise direction with 1, 2 and 3, then the expression for the shape function associated with the node 1 is given as

$$N_1 = \frac{1}{2\Delta}[(x_2y_3 - x_3y_2) + (y_2 - y_3)x + (x_3 - x_2)y] \tag{4}$$

where Δ represents the elemental area, i.e. $\Delta = 0.5|(x_1 - x_3)(y_2 - y_3) - (x_3 - x_2)(y_3 - y_1)|$. For rest of the two nodes, the shape functions can further be defined by following the same pattern.

The statically admissible stress discontinuities in between adjoining elements are permitted in the LB FELA. The discontinuous stress field generates additional degrees of freedom which help to improve the LB solution significantly (Sloan, 1988; Pastor, 2003).

Fig. 1b presents a typical mesh used in the analysis. Note that the sizes of the elements gradually decrease as it approaches towards the edges of the strip footing. To simulate the singularity of stress at the footing edge, a fan type of the mesh is chosen along the edges of the footing. The horizontal and vertical extents of the semi-circular domain (UVR), denoted by L_h and L_v, respectively, are kept sufficiently large so that the proximity of the stresses near the edge of the boundaries remains far away from the yield. It is also ensured that the magnitude of the collapse load remains unchanged even if the chosen boundaries of the domain are extended further.

4.2. LB formulation

As per the theory of the plasticity, the LB solution is achieved from a statically admissible stress field which satisfies equilibrium conditions everywhere in the domain and stress boundary conditions and it nowhere violates the yield criterion (Sloan, 1988).

4.2.1. Equilibrium equation

As the rock media are subjected to horizontal pseudo-static seismic acceleration k_h, the equilibrium of each element must be satisfied using the following equations:

$$\frac{\partial \sigma_x}{\partial x} + \frac{\partial \tau_{xy}}{\partial y} = k_h \gamma \tag{5a}$$

$$\frac{\partial \sigma_y}{\partial y} + \frac{\partial \tau_{xy}}{\partial x} = \gamma \tag{5b}$$

Note that the pseudo-static horizontal seismic body forces are incorporated in the analysis with the application of Eq. (5a). For $k_h = 0$, the term on the right hand side of equal sign in Eq. (5a) becomes simply equal to zero. Substituting Eq. (3) into Eq. (5) will lead to the following equality constraint(s):

$$\boldsymbol{A}_{\text{equi}}\overline{\boldsymbol{\sigma}} = \boldsymbol{b}_{\text{equi}} \tag{6}$$

where $\boldsymbol{A}_{\text{equi}}$ and $\boldsymbol{b}_{\text{equi}}$ represent the matrix and vector associated with the equilibrium conditions, respectively; and $\overline{\boldsymbol{\sigma}}$ comprises the global vector of unknown stresses at the nodes.

4.2.2. Stress discontinuities

The continuities of normal and shear stresses are maintained along the interfaces of all the elements. Along the interface of any two adjacent elements i and j, with the nodal pairs (1, 2) and (3, 4), the following conditions must hold good:

$$\sigma_{n,1} = \sigma_{n,2}, \tau_{tn,1} = \tau_{tn,2}, \sigma_{n,3} = \sigma_{n,4}, \tau_{tn,3} = \tau_{tn,4} \tag{7}$$

where subscripts n and tn represent the normal and tangential directions, respectively, along the discontinuity line. The nodes 1 and 3 are associated with the element i, and the nodes 2 and 4 form a part of the element j. This will result in the generation of the following equality constraints:

$$\boldsymbol{A}_{\text{sd}}\overline{\boldsymbol{\sigma}} = \boldsymbol{b}_{\text{sd}} \tag{8}$$

where $\boldsymbol{A}_{\text{sd}}$ and $\boldsymbol{b}_{\text{sd}}$ represent the matrix and vector associated with the continuity of the stresses along the interface (discontinuity line) of the two adjoining elements.

It should be mentioned that the state of stress for any plane strain problem can be defined with the usage of three stress variables. The continuity of the normal and shear stresses only ensures the equal values of the two of the three stress variables on either side of the stress discontinuity. The difference in the value of the third stress variable makes the stress state different on either side of the stress discontinuity.

4.2.3. Boundary conditions

The boundary conditions applicable for this problem are shown in Fig. 1a, in which ST denotes the base of the footing. Note that at failure, the vertical load on the footing is Q_u and the horizontal shear force is $k_h Q_u$. The extent of the semi-circular periphery (UVR) is kept sufficiently large, and it is ensured, like everywhere within the problem domain, the GHB yield condition is nowhere violated along this boundary.

(1) Boundary conditions along the ground surface

A vertical surcharge of q_0 is applied over ground surface either side of the footing, i.e. along the boundaries RS and TU. Therefore, the vertical normal stress (σ_n) along these boundaries will be simply equal to the applied surcharge pressure (q_0). Due to horizontal inertial seismic force, a shear stress of $k_h q_0$ will develop along these boundaries. Hence, the following boundary stresses need to be enforced along the boundaries RS and TU:

$$\sigma_n = q_0, \ \tau = k_h q_0 \tag{9}$$

(2) Boundary conditions along the footing-rock interface

Since the footing is assumed to be rough, the yield strength of the footing-rock interface is assumed to be the same as that of the yield strength of the rock medium. Therefore, no exclusive constraint on the shear stress needs to be imposed for any node along the footing-rock interface. However, the effect of the horizontal inertial force due to the overlying mass of the superstructure is incorporated by introducing the following equality constraint along the footing-rock interface:

$$Q_h = k_h Q_u \tag{10}$$

where $Q_u = \int_A \sigma_y dx$ and $Q_h = \int_A \tau_{xy} dx$, in which A denotes the area of the strip footing. This implies that the resultant load on the footing becomes inclined with the vertical inclination of the resultant load at an angle $\tan^{-1} k_h$

The imposition of the stress boundary conditions can be specified by the following condition:

$$\boldsymbol{A}_{\text{bc}}\overline{\boldsymbol{\sigma}} = \boldsymbol{b}_{\text{bc}} \tag{11}$$

where $\boldsymbol{A}_{\text{bc}}$ and $\boldsymbol{b}_{\text{bc}}$ represent the matrix and vector in connection with the applied boundary conditions, respectively.

4.2.4. Imposition of the yield condition

The GHB yield criterion, as defined by Eq. (1), can be expressed as

$$\sigma_1 - \sigma_3 \le (p\sigma_1 + r)^{\alpha} \tag{12}$$

where $p = -m_b(-\sigma_{ci})^{(1-\alpha)/\alpha}$ and $r = s(-\sigma_{ci})^{1/\alpha}$.

Introducing a new variable t such that

$$t = (p\sigma_1 + r)^{\alpha} \tag{13}$$

Since $\sigma_1 > \sigma_3$ and $t \ge 0$, hence, Eq. (12) can be re-written as

$$\sigma_1 - \sigma_3 \le t \tag{14}$$

For a plane strain problem, we have

$$\sigma_1 = \frac{\sigma_x + \sigma_y}{2} + \sqrt{\left(\frac{\sigma_x - \sigma_y}{2}\right)^2 + \tau_{xy}^2} \tag{15a}$$

$$\sigma_3 = \frac{\sigma_x + \sigma_y}{2} - \sqrt{\left(\frac{\sigma_x - \sigma_y}{2}\right)^2 + \tau_{xy}^2} \tag{15b}$$

Therefore, Eq. (14), after substituting Eqs. (15a) and (15b), can be written as

$$\sqrt{(\sigma_x - \sigma_y)^2 + (2\tau_{xy})^2} \le t \tag{16}$$

Since $t \geq 0$, Eq. (16) can easily be expressed in the standard form of a second order conic constraint:

$$\sqrt{x_2^2 + x_3^2} \leq x_1 \tag{17}$$

where $x_1 = t$, $x_2 = (\sigma_x - \sigma_y)$ and $x_3 = 2\tau_{xy}$.

For a plane strain case problem, using Eq. (15a), the value of t in Eq. (13) can be written in terms of σ_x, σ_y and τ_{xy}:

$$t = \left\{ \frac{p}{2} \left[(\sigma_x + \sigma_y) + \sqrt{(\sigma_x - \sigma_y)^2 + (2\tau_{xy})^2} \right] + r \right\}^{\alpha} \tag{18}$$

Since the value of the exponent α is always positive, using Eqs. (16) and (18), it can be written as

$$t \leq \left\{ \frac{p}{2} \left[(\sigma_x + \sigma_y) + t \right] + r \right\}^{\alpha} \tag{19}$$

If x_4, x_5 and x_6 are defined by the following expressions:

$$x_4 = \frac{p}{2} \left[(\sigma_x + \sigma_y) + t \right] + r,\ x_5 = 1,\ x_6 = t \tag{20}$$

Then, Eq. (19) will take the form of a power conic constraint as defined by

$$\sqrt{x_6^2} \leq x_4^{\alpha} x_5^{1-\alpha} \tag{21}$$

Note that the variable x_4 needs to be always positive.

Accordingly, the optimization problem in the LB FELA can be solved by imposing the GHB failure criterion as the summation of one quadratic conic constraint (Eq. (17)) and one power conic constraint (Eq. (21)).

It should be mentioned that an n-dimensional power cone can be defined as

$$\wp^n = \left\{ \boldsymbol{u} \in \Re^n \;\middle|\; u_1^{\alpha}\, u_2^{1-\alpha} \geq \sqrt{u_3^2 + u_4^2 + \ldots + u_n^2} \right\} (\, u_1,\ u_2 \geq 0 \text{ and } 0 < \alpha < 1) \tag{22a}$$

In the present formulation, the following form of the 3D power cone has been considered:

$$\sqrt{u_3^2} \leq u_1^{\alpha}\, u_2^{1-\alpha} (u_1,\ u_2 \geq 0 \text{ and } 0 < \alpha < 1) \tag{22b}$$

This form of the GHB yield constraint has already been indicated in Eq. (21) with $u_3 = x_6$, $u_1 = x_4$ and $u_2 = x_5$.

4.3. The optimization problem

Finally, all the constraints were assembled to maximize the objective function, i.e. the magnitude of the collapse load, by forming the following canonical form of the optimization problem:

$$\text{Maximize } \boldsymbol{c}^{\mathrm{T}} \boldsymbol{\sigma} \tag{23a}$$

$$\text{Subjected to } \boldsymbol{A}_{\mathrm{eq}} \boldsymbol{\sigma} = \boldsymbol{b}_{\mathrm{eq}},\ \boldsymbol{A}_{\mathrm{cone}} \boldsymbol{\sigma} + \boldsymbol{x}_{\mathrm{cone}} = \boldsymbol{b}_{\mathrm{cone}} \tag{23b}$$

where $\boldsymbol{c}$ is the vector containing the coefficients of the objective function; $\boldsymbol{A}_{\mathrm{eq}}$ is the matrix containing the coefficients of all the equality constraints as expressed in Eqs. (6), (8) and (11); $\boldsymbol{b}_{\mathrm{eq}}$ is corresponding right known vector of the equality constraints; $\boldsymbol{A}_{\mathrm{cone}}$ is the matrix containing the coefficients of all the conic constraints, and $\boldsymbol{b}_{\mathrm{cone}}$ is the corresponding right known vector of the conic constraints. If the total number of nodes is denoted by NN, the vectors $\boldsymbol{\sigma}$ and $\boldsymbol{x}_{\mathrm{cone}}$ are defined as

$$\boldsymbol{\sigma}^{\mathrm{T}} = \left\{ \sigma_x^1\ \sigma_y^1\ \tau_{xy}^1\ t^1, \ldots, \sigma_x^i\ \sigma_y^i\ \tau_{xy}^i\ t^i, \ldots, \sigma_x^{NN}\ \sigma_y^{NN}\ \tau_{xy}^{NN}\ t^{NN} \right\} \tag{24a}$$

$$\boldsymbol{x}_{\mathrm{cone}}^{\mathrm{T}} = \left\{ x_1^1\ x_2^1\ x_3^1\ x_4^1\ x_5^1\ x_6^1, \ldots, x_1^i\ x_2^i\ x_3^i\ x_4^i\ x_5^i\ x_6^i, \ldots, x_1^{NN}\ x_2^{NN}\ x_3^{NN}\ x_4^{NN}\ x_5^{NN}\ x_6^{NN} \right\} \tag{24b}$$

where σ_x^i, σ_y^i and τ_{xy}^i represent the stresses; t^i refers to the slack variable at the node i; and x_1^i, x_2^i, x_3^i, x_4^i, x_5^i and x_6^i are the conic variables corresponding to the node i. Note that the equality constraint in the second equation of Eq. (23b) is the combination of Eqs. (17) and (21), obtained from the conic representation of the GHB criterion.

The computer code to perform the LB FELA with the usage of the GHB was written in MATLAB. For this large-scale conic optimization problem, the solver MOSEK, which is based on the primal-dual interior-point method (Andersion et al., 2003) and has already been recommended by a number of researchers (Martin and Makrodimopoulos, 2008; Tang et al., 2014; Kumar and Mohapatra, 2017; Ukritchon and Keawsawasvong, 2018) because of its robustness and computational efficiency, was used in the present analysis. The computations were carried out on a desktop computer (Intel Core i7–7700 K CPU @ 4.20 GHz, 16 GB RAM) in the Windows 10 operating-based system.

5. Results and discussions

5.1. Bearing capacity equation

Similar to Terzaghi (1943)'s bearing capacity equation for a footing resting on a soil medium, the following equation is used to determine the ultimate bearing capacity ($q_{\mathrm{u}} = Q_{\mathrm{u}}/A$) of a strip footing placed on rock mass:

$$q_{\mathrm{u}} = \sigma_{\mathrm{ci}} N_{\sigma} + q_0 N_q \tag{25}$$

where N_{σ} and N_q refer to the non-dimensional bearing capacity factors associated with the self-weight of rock mass and surcharge pressure, respectively. Deriving the bearing capacity factor (N_{σ}) due to unit weight of the rock mass requires surcharge pressure to be zero ($q_0 = 0$), thus it is calculated as

$$N_{\sigma} = \frac{q_{\mathrm{u}}}{\sigma_{\mathrm{ci}}} \tag{26}$$

If the rock mass is considered to be weightless, then the bearing capacity factor N_{σ} is termed as $N_{\sigma 0}$.

The bearing capacity factor due to surcharge (N_q) can be expressed as

$$N_q = \frac{q_{\mathrm{u}} - \sigma_{\mathrm{ci}} N_{\sigma}}{q_0} \tag{27}$$

The bearing capacity factors for different seismic coefficients (k_{h}), ranging from 0.0 to 0.5 (Terzaghi, 1950), have been computed and the final results are presented in both graphical and tabular forms for all the practical range of the Hoek-Brown parameters as mentioned in the earlier section. The effects of γ and q_0 on bearing capacity factors have been examined in the form of dimensionless parameters $\sigma_{\mathrm{ci}}/(\gamma B)$ and q_0/σ_{ci}. The value of $\sigma_{\mathrm{ci}}/(\gamma B)$ is varied from 100 to infinity (inf); the infinite value of $\sigma_{\mathrm{ci}}/(\gamma B)$ implies a zero value of the unit weight. The value of q_0/σ_{ci} was varied from 0 to 1.

It should be noted that the rock mass in this study is considered to be an undisturbed ($D = 0$) one.

5.2. Validation of the present analysis

The present analysis has been validated by comparing the obtained solution with that reported in the literature. The comparison of the results has been carried out for the static case as well with the consideration of the pseudo-static inertial forces. On account of non-availability of the results, at present, no comparison could be, however, made for the true dynamic case; this will form the scope of the future study.

5.2.1. Comparison for static case

The accuracy of the present solutions is verified by comparing the bearing capacity factor $N_{\sigma 0}$ for a weightless rock medium with the available results of Kulhawy and Carter (1992) using the LB analysis but with an assumption of the collapse mechanism, Serrano et al. (2000) on the basis of the slip line method, Merifield et al. (2006) using the average of the LB and UB solutions using the nonlinear optimization, and the LB solution of Chakraborty and Kumar (2015). The comparisons of all these results are shown in Table 1 for $k_h = 0$. The bearing capacity factors proposed by Kulhawy and Carter (1992) from the simplified LB solutions are always found to be remarkably lower than all the other reported solutions. The slip-line solutions estimated by Serrano et al. (2000) are found to be quite close to the present FELA solutions and the difference between the two solutions is found to be very nominal. The present LB solutions are also found to match well with the average of the LB and UB solutions of Merifield et al. (2006), and the LB solutions of Chakraborty and Kumar (2015). The studies of Merifield et al. (2006) and Chakraborty and Kumar (2015) are based on the FELA technique using the nonlinear programming.

Table 1
A comparison of the bearing capacity factor for a weightless rock mass in the absence of surcharge with $k_h = 0$.

GSI	m_i	Bearing capacity factor of weightless media, $N_{\sigma 0}$				
		Kulhawy and Carter (1992)[a]	Serrano et al. (2000)[b]	Merifield et al. (2006)[c]	Chakraborty and Kumar (2015)[d]	Present analysis[e]
10	5	0.016	0.035	0.042	0.04	0.042
	10	0.022	0.072	0.077	0.075	0.077
	20	0.032	0.159	0.156	0.151	0.153
	30	0.039	0.259	0.238	0.23	0.237
	35	0.043	0.314	0.288	0.276	0.282
30	5	0.095	0.227	0.235	0.23	0.234
	10	0.127	0.393	0.397	0.388	0.395
	20	0.174	0.716	0.713	0.701	0.705
	30	0.21	1.038	1.022	1.015	1.011
	35	0.226	1.2	1.193	1.182	1.164
50	5	0.29	0.638	0.644	0.631	0.642
	10	0.38	1.031	1.037	1.028	1.032
	20	0.51	1.76	1.765	1.739	1.752
	30	0.61	2.458	2.467	2.406	2.439
	35	0.654	2.801	2.817	2.766	2.776
70	5	0.785	1.574	1.582	1.571	1.576
	10	1.012	2.434	2.444	2.415	2.433
	20	1.339	3.998	4.012	3.978	3.986
	30	1.592	5.47	5.491	5.437	5.447
	35	1.703	6.187	6.068	6.036	6.156
100	5	3.449	6.114	6.124	6.095	6.101
	10	4.317	8.875	8.896	8.798	8.86
	20	5.583	13.809	13.847	13.789	13.78
	30	6.568	18.39	18.444	18.398	18.341
	35	7	20.628	20.688	20.587	20.543

[a] Simple analytical LB solution.
[b] Slip-line solution.
[c] Average of LB and UB FELA solutions using nonlinear programing.
[d] LB FELA solution using nonlinear programing.
[e] LB FELA solution using power cone programing.

5.2.2. Comparison for pseudo-static case

For $\gamma = 0$, $q_0 = 0$ and $k_h = 0$–0.2, Table 2 provides a comparison of the present results with the existing solution of Saada et al. (2011) on the basis of the kinematic limit analysis approach with the incorporation of the pseudo-static inertial forces. It can be noted that the values of $N_{\sigma 0}$ reported by Saada et al. (2011) are found to be marginally greater than the present LB solution; it is quite an expected outcome since the present analysis is based on the application of the LB limit theorem.

5.3. The variation of the bearing capacity factors with k_h

The variation of the bearing capacity factor $N_{\sigma 0}$ for a weightless rock medium with respect to changes in k_h, ranging from 0 to 0.5, is illustrated in Fig. 2. This figure displays the variation of $N_{\sigma 0}$ for seven different values of m_i ranging from 5 to 35, with an interval of 5, and six different values of *GSI*, i.e. 10, 20, 40, 60, 80 and 100. It can be clearly noted that the magnitude of $N_{\sigma 0}$ decreases continuously with an increase in the value of k_h. For $GSI = 10$ and $m_i = 5$, with an increase in k_h from 0 to 0.2, the factor $N_{\sigma 0}$ decreases by 30.14%, and from 0.2 to 0.4, the factor $N_{\sigma 0}$ decreases by 35.96%. Similarly, for $GSI = 10$ and $m_i = 30$, with an increase in k_h from 0 to 0.2, the factor $N_{\sigma 0}$ decreases by 33.77%, and from 0.2 to 0.4, the factor $N_{\sigma 0}$ decreases by 38.77%. Furthermore, for $GSI = 80$ and $m_i = 5$, with an increase in k_h from 0 to 0.2, the factor $N_{\sigma 0}$ decreases by 27.54%, and from 0.2 to 0.4, the factor $N_{\sigma 0}$ decreases by 33.89%.

Figs. 3 and 4 display the variation of the bearing capacity factor N_σ with the changes in k_h for $\sigma_{ci}/(\gamma B) = 100$ and 1000, respectively. Four different sub-plots are meant for four different values of *GSI*, i.e. 20, 40, 60 and 80. It can be seen that in all the cases, the value of the factor N_σ reduces invariably with an increase in the value of k_h.

Table 2
A comparison of the bearing capacity factor for $\gamma = 0$ and $q_0 = 0$ with $k_h \geq 0$.

m_i	*GSI*	Bearing capacity factor of weightless media, $N_{\sigma 0}$					
		$k_h = 0$		$k_h = 0.1$		$k_h = 0.2$	
		Saada et al. (2011)[a]	Present analysis[b]	Saada et al. (2011)[a]	Present analysis[b]	Saada et al. (2011)[a]	Present analysis[b]
10	10	0.0779	0.0769	0.065	0.0643	0.053	0.0525
	20	0.2097	0.2071	0.1765	0.1747	0.1449	0.1437
	30	0.3996	0.395	0.3378	0.3348	0.2788	0.2767
	40	0.6632	0.6563	0.5627	0.558	0.466	0.4628
	50	1.0416	1.0319	0.8861	0.8795	0.7356	0.7311
	60	1.6027	1.5891	1.3663	1.3572	1.1366	1.1305
	70	2.452	2.4329	2.0946	2.082	1.7454	1.7371
	80	3.7544	3.7267	3.2136	3.1962	2.6823	2.6709
15	10	0.116	0.1142	0.0962	0.0949	0.0779	0.077
	20	0.3008	0.2962	0.2518	0.2487	0.2059	0.2037
	30	0.5588	0.5511	0.4708	0.4654	0.3871	0.3834
	40	0.9118	0.9005	0.7709	0.7632	0.6364	0.6309
	50	1.4139	1.3979	1.1988	1.1876	0.9917	0.9843
	60	2.1522	2.1292	1.8282	1.8127	1.5161	1.5052
	70	3.2581	3.2269	2.7727	2.7519	2.3024	2.2892
	80	4.9379	4.8921	4.2104	4.181	3.5026	3.4834
25	10	0.1985	0.1945	0.1634	0.1606	0.1314	0.1294
	20	0.4863	0.4773	0.4052	0.3987	0.3296	0.325
	30	0.8734	0.8585	0.7326	0.722	0.5999	0.5924
	40	1.3945	1.3728	1.1744	1.159	0.9653	0.9546
	50	2.1283	2.0981	1.7969	1.7759	1.4817	1.4665
	60	3.1969	3.1551	2.7049	2.6758	2.2345	2.214
	70	4.7823	4.7236	4.0533	4.0125	3.3544	3.3268
	80	7.1632	7.0809	6.0834	6.0269	5.0399	5.0009

[a] UB kinematic limit analysis.
[b] LB FELA.

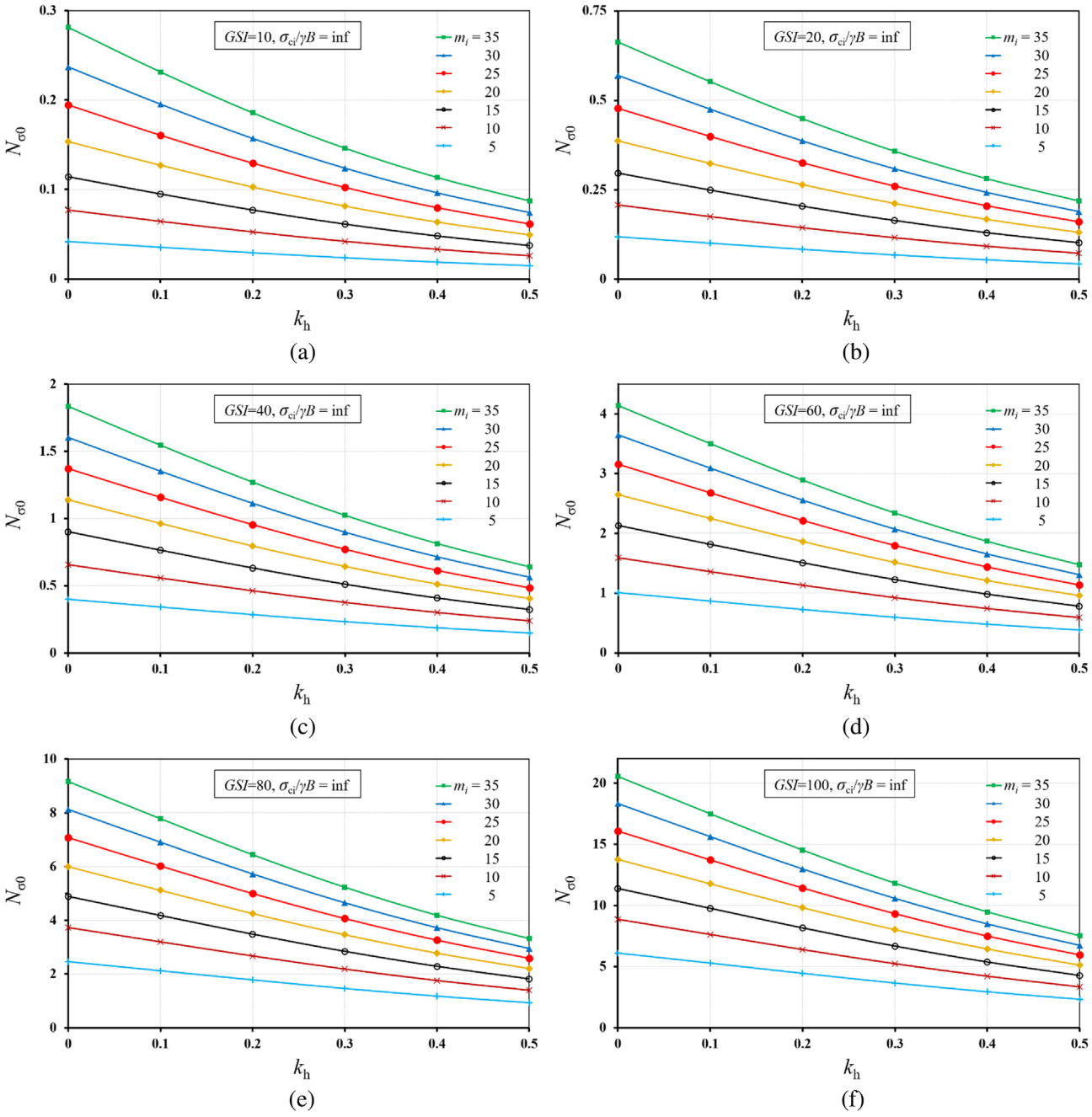

Fig. 2. Variation of $N_{\sigma 0}$ with k_h for different m_i values and (a) *GSI* =10, (b) *GSI* =20, (c) *GSI* =40, (d) *GSI* =60, (e) *GSI* = 80, and (f) *GSI* = 100.

To examine the effect of surcharge (q_0) on the bearing capacity factor, several computations have been performed and these results have been presented in Figs. 5–13 in terms of the variation of the factor N_q with an increase in the value of k_h. Similar to N_σ, a significant reduction in N_q with an increase in k_h is observed. For example, in case of $\sigma_{ci}/(\gamma B)$= inf, q_0/σ_{ci} = 0.25 and m_i = 20, if the value of k_h changes from 0 to 0.3, the corresponding magnitude of N_q decreases by 49.22% and 45.06% corresponding to the value of *GSI* equal to 20 and 60, respectively. Fig. 5 has been drawn to bring out the effect of $\sigma_{ci}/(\gamma B)$ on the variation of N_q with changes in k_h. Three different values of $\sigma_{ci}/(\gamma B)$, i.e. 100, 1000 and infinity ($\gamma = 0$) have been used. Note that the magnitude of N_q increases marginally with an increase in $\sigma_{ci}/(\gamma B)$. The difference in the values of N_q for $\sigma_{ci}/(\gamma B)$ = 1000 and inf has been found to be much smaller than the corresponding difference between the values of N_q for $\sigma_{ci}/(\gamma B)$ = 100 and 1000. The variation of N_q for $\sigma_{ci}/(\gamma B)$=100, q_0/σ_{ci}= 0.25, with respect to k_h for different values of m_i between 5 and 35, and *GSI* between 20 and 80 is shown in Fig. 6. Likewise, Figs. 7–9 present the results for $\sigma_{ci}/(\gamma B)$=100 corresponding to the value of q_0/σ_{ci} equal to 0.5, 0.75 and 1, respectively. Note that the magnitude of N_q decreases marginally with an increase q_0/σ_{ci}, it should be mentioned that the product q_0N_q always increases with an increase in q_0/σ_{ci}. The magnitude of N_q increases continuously with increases in m_i and *GSI*. Figs. 10–13 provide the variation of N_q with an increase in k_h for $\sigma_{ci}/(\gamma B)$= inf corresponding to q_0/σ_{ci} equal to 0.25, 0.5, 0.75 and 1, respectively. As indicated earlier, the

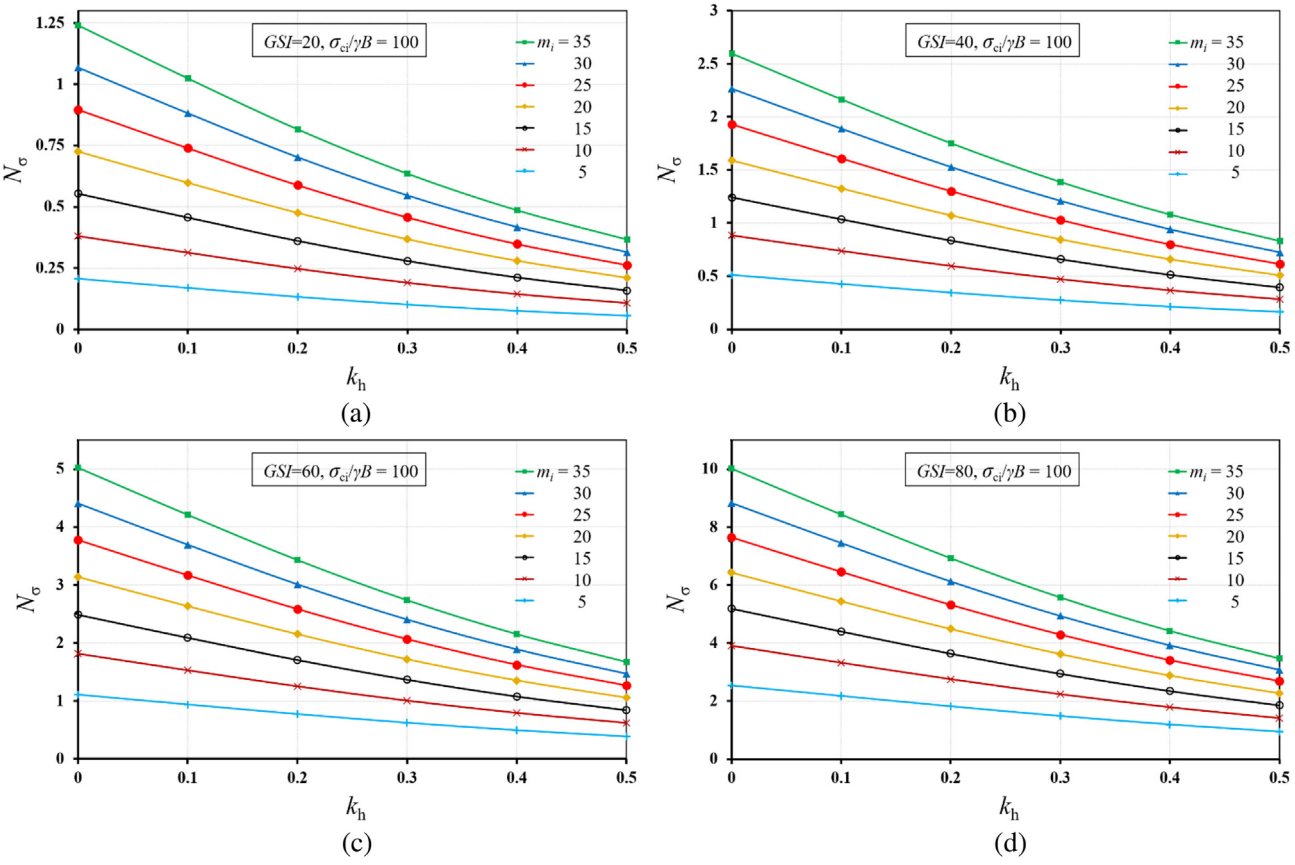

Fig. 3. Variation of N_σ with k_h for different m_i values with (a) $GSI = 20$, (b) $GSI = 40$, (c) $GSI = 60$, and (d) $GSI = 80$.

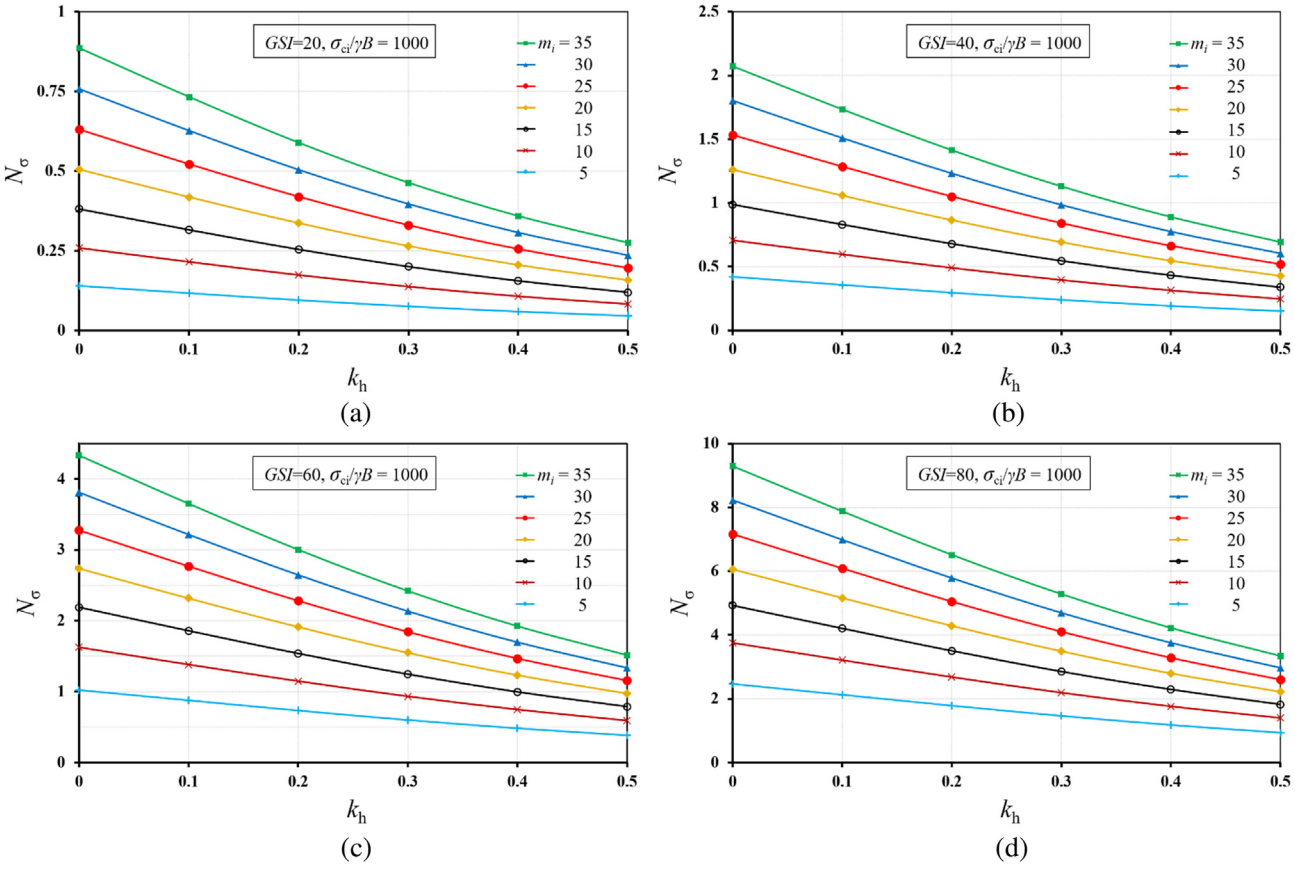

Fig. 4. Variation of N_σ with k_h for $\sigma_{ci}/(\gamma B) = 1000$ for different m_i values with (a) $GSI = 20$, (b) $GSI = 40$, (c) $GSI = 60$, and (d) $GSI = 80$.

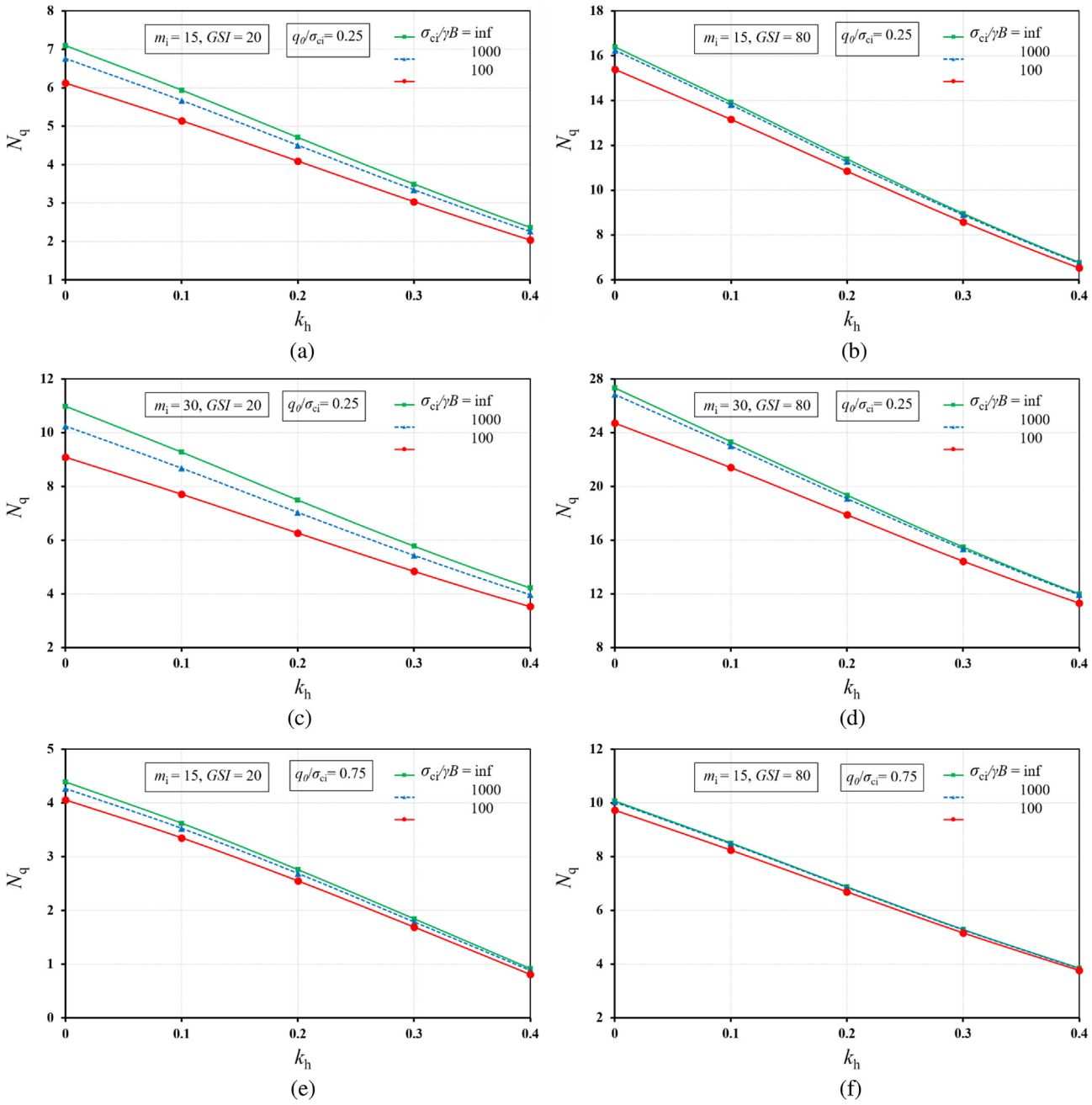

Fig. 5. Effect of $\sigma_{ci}/(\gamma B)$ on N_q with changes in k_h for (a) m_i=15, *GSI*=20 and q_0/σ_{ci}= 0.25; (b) m_i=15, *GSI*=80 and q_0/σ_{ci}= 0.25; (c) m_i=30, *GSI*=20 and q_0/σ_{ci}= 0.25; (d) m_i=30, *GSI*=80 and q_0/σ_{ci}= 0.25; (e) m_i=15, *GSI*=20 and q_0/σ_{ci}= 0.75; and (f) m_i=15, *GSI*=80 and q_0/σ_{ci}= 0.75.

magnitude of N_q for $\sigma_{ci}/(\gamma B)$=inf becomes marginally greater than that with $\sigma_{ci}/(\gamma B) = 100$.

5.4. Failure patterns

In order to investigate how the failure patterns are influenced by the variation in the seismic coefficient with and without the presence of surcharge pressure, the proximity of the stress state to failure was defined in terms of a non-dimensional ratio, a/b, where $a = (\sigma_1 - \sigma_3)$ and $b = (p\sigma_1 + r)^{\alpha}$. This ratio is defined in a way such that it will attain a maximum value of 1 when the point is in the state of yield, otherwise, it will have a value smaller than unity for a non-yielded stress state. The failure patterns are shown in Figs. 14 and 15. With $\sigma_{ci}/(\gamma B) = 100$, Fig. 14 illustrates the failure patterns, without any surcharge pressure, for different values of k_h, i.e. 0, 0.02, 0.05 and 0.1 with $GSI = 30$, $m_i = 5$, and $GSI = 80$, $m_i = 15$. For $k_h = 0$, the failure patterns become symmetrical about the center line passing through the footing base. In the presence of k_h, the pattern becomes unsymmetrical. With an increase in k_h, the extent of the plastic zone on one side of the footing, both horizontally and vertically, reduces continuously. The extent of the plastic zone for larger values of *GSI* and m_i becomes continuously greater. Fig. 15 illustrates the effect of surcharge on the shape of the yielded zone for different values of *GSI*, m_i and k_h and q_0/σ_{ci}=0.5 and 1. Once again, an introduction to the seismic force produces a non-

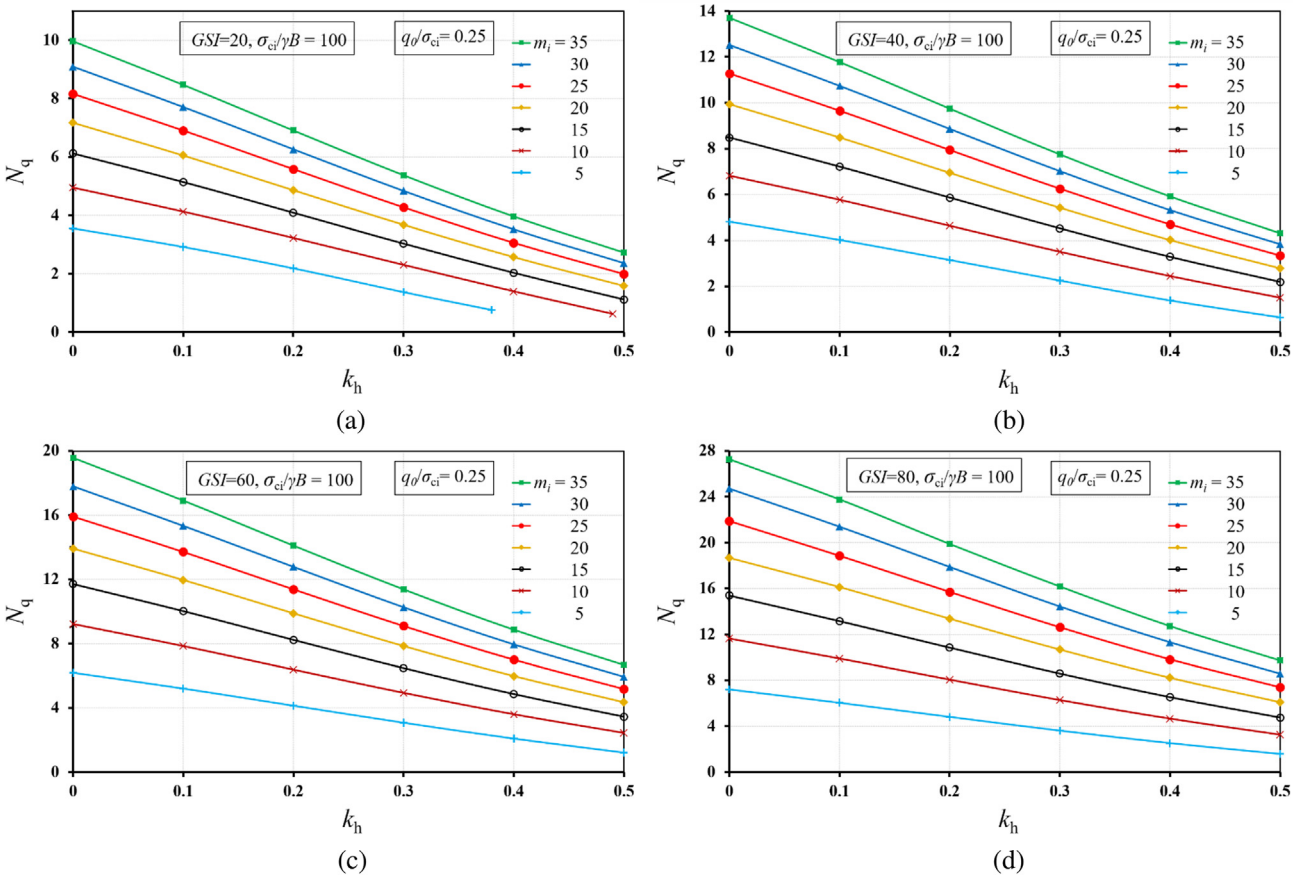

Fig. 6. Variation of N_q with k_h for $\sigma_{ci}/(\gamma B)$=100, q_0/σ_{ci}= 0.25 for different m_i values with (a) *GSI* = 20, (b) *GSI* = 40, (c) *GSI* = 60, and (d) *GSI* = 80.

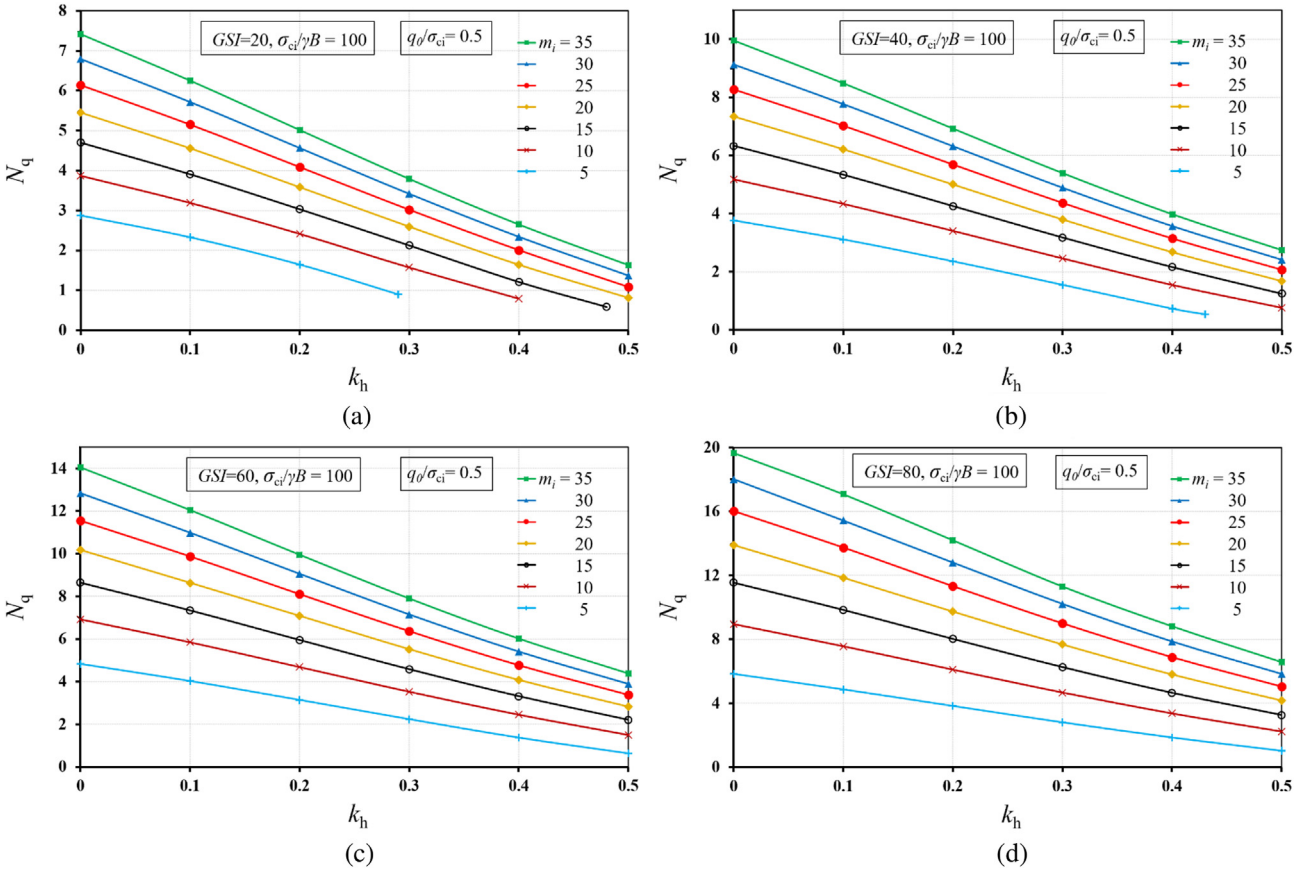

Fig. 7. Variation of N_q with k_h for $\sigma_{ci}/(\gamma B)$=100 and q_0/σ_{ci}= 0.5 for different m_i with (a) *GSI* = 20, (b) *GSI* = 40, (c) *GSI* = 60, and (d) *GSI* = 80.

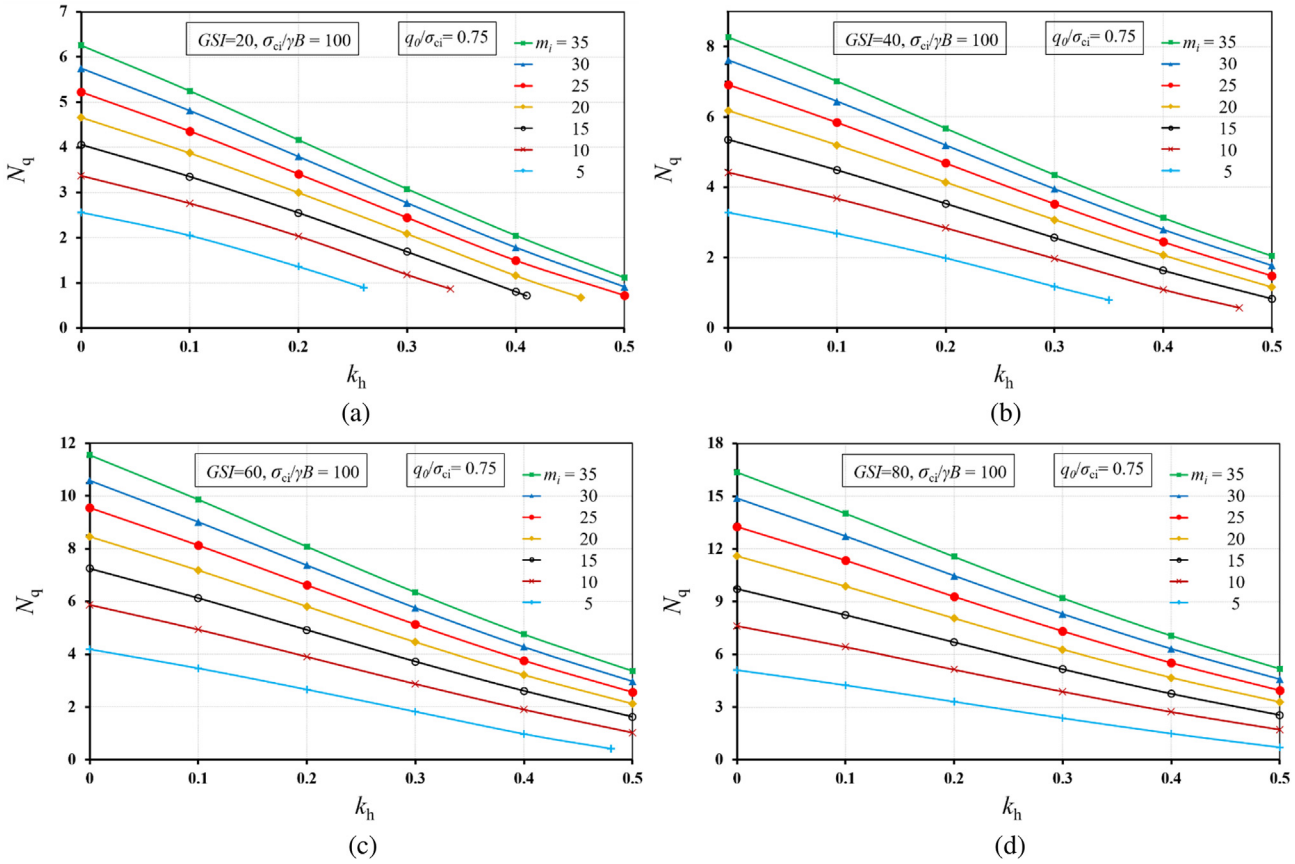

Fig. 8. Variation of N_q with k_h for $\sigma_{ci}/(\gamma B)$=100 and q_0/σ_{ci}= 0.75 for different m_i with (a) *GSI* = 20, (b) *GSI* = 40, (c) *GSI* = 60, and (d) *GSI* = 80.

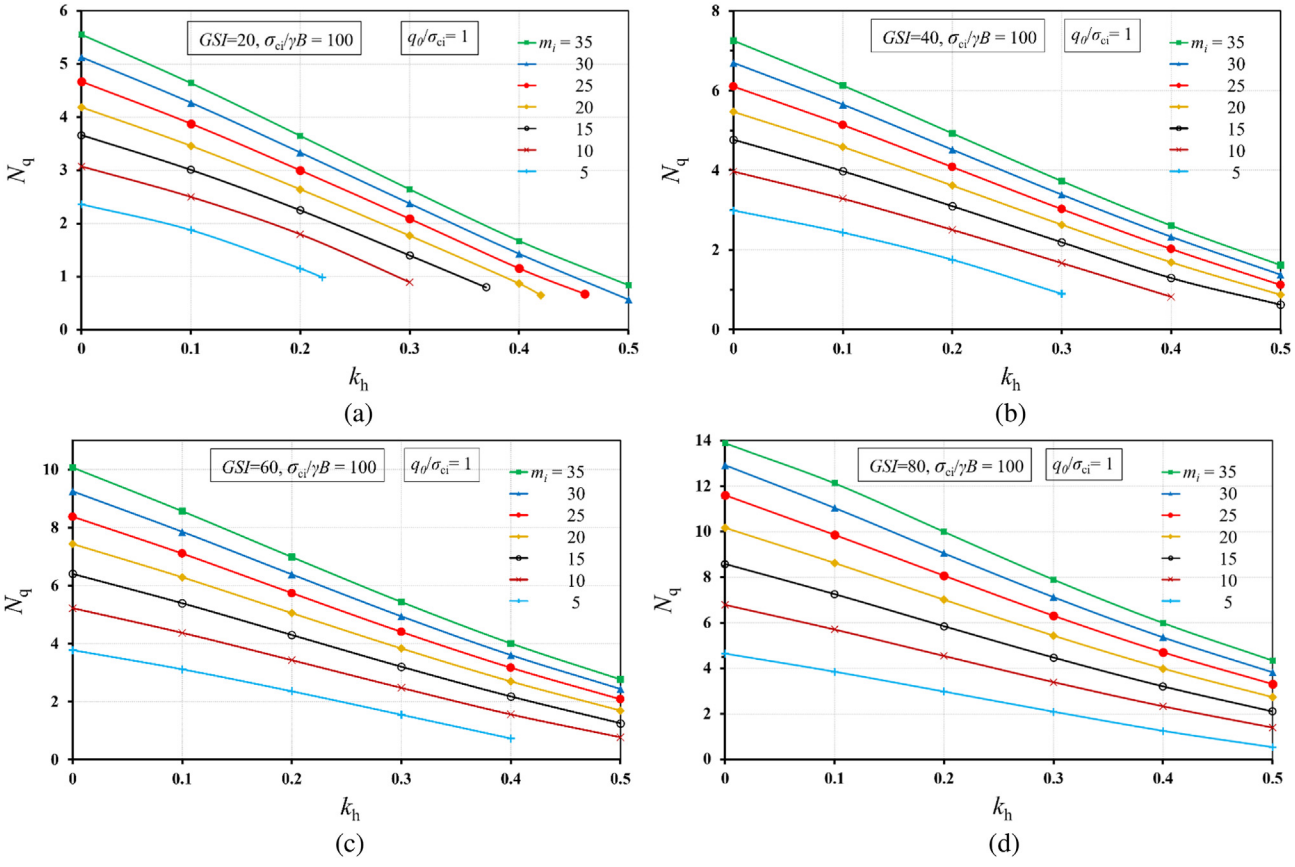

Fig. 9. Variation of N_q with k_h for $\sigma_{ci}/(\gamma B)$=100 and q_0/σ_{ci}= 1 for different m_i with (a) *GSI* = 20, (b) *GSI* = 40, (c) *GSI* = 60, and (d) *GSI* = 80.

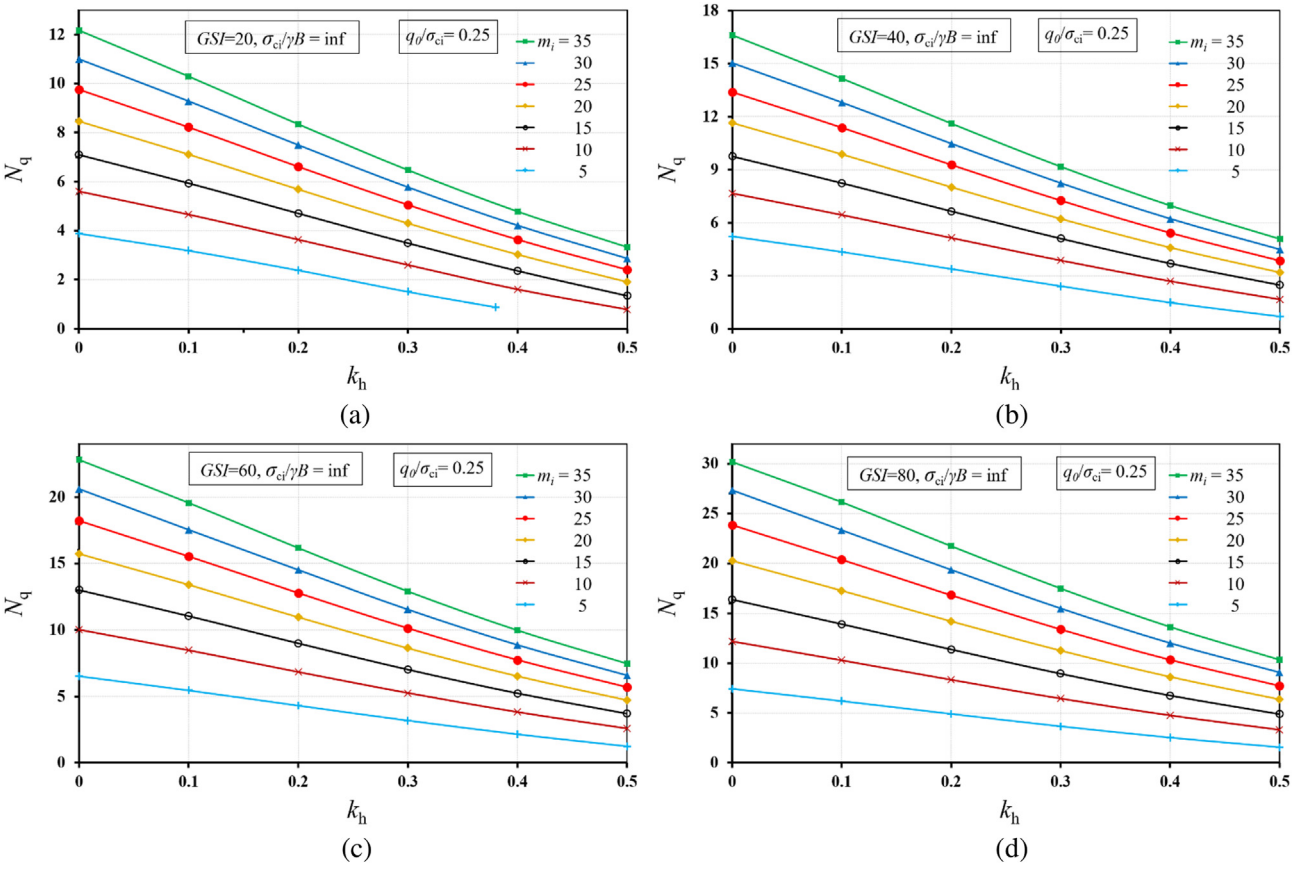

Fig. 10. Variation of N_q with k_h for $\sigma_{ci}/(\gamma B)$= inf and q_0/σ_{ci}= 0.25 for different m_i values with (a) $GSI = 20$, (b) $GSI = 40$, (c) $GSI = 60$, and (d) $GSI = 80$.

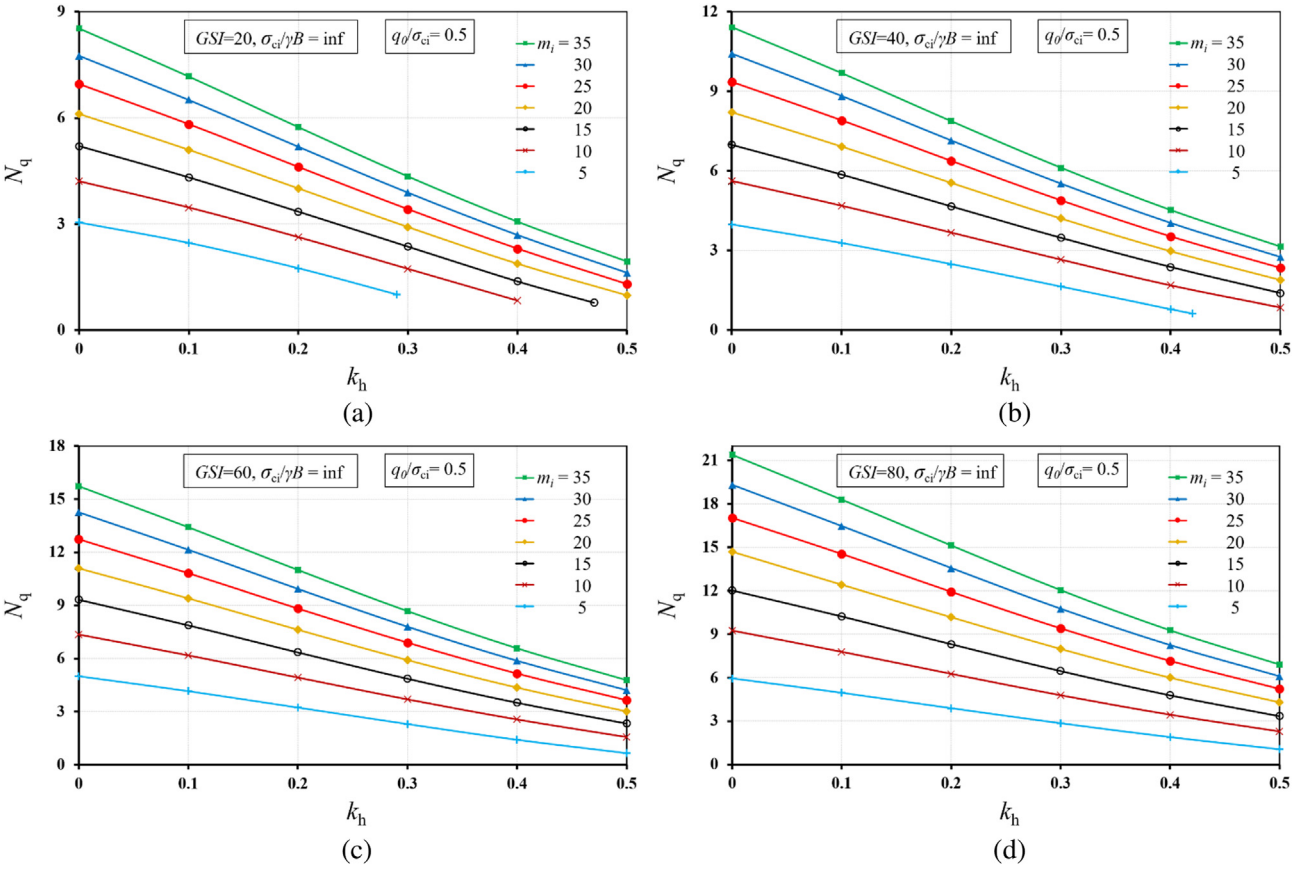

Fig. 11. Variation of N_q with k_h for $\sigma_{ci}/(\gamma B)$= inf and q_0/σ_{ci}= 0.5 for different m_i values with (a) $GSI = 20$, (b) $GSI = 40$, (c) $GSI = 60$, and (d) $GSI = 80$.

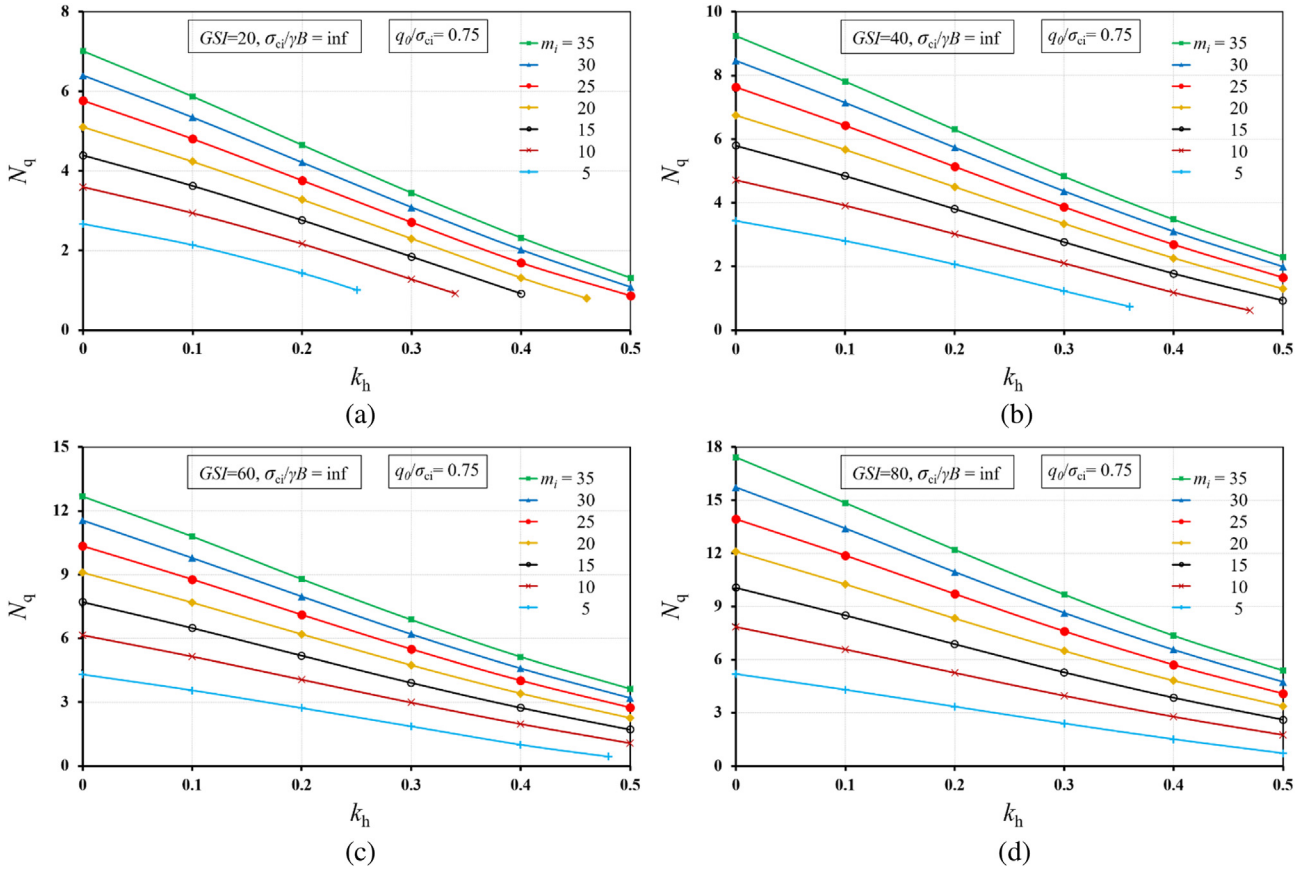

Fig. 12. Variation of N_q with k_h for $\sigma_{ci}/(\gamma B)$= inf and q_0/σ_{ci}= 0.75 for different m_i values with (a) *GSI* = 20, (b) *GSI* = 40, (c) *GSI* = 60, and (d) *GSI* = 80.

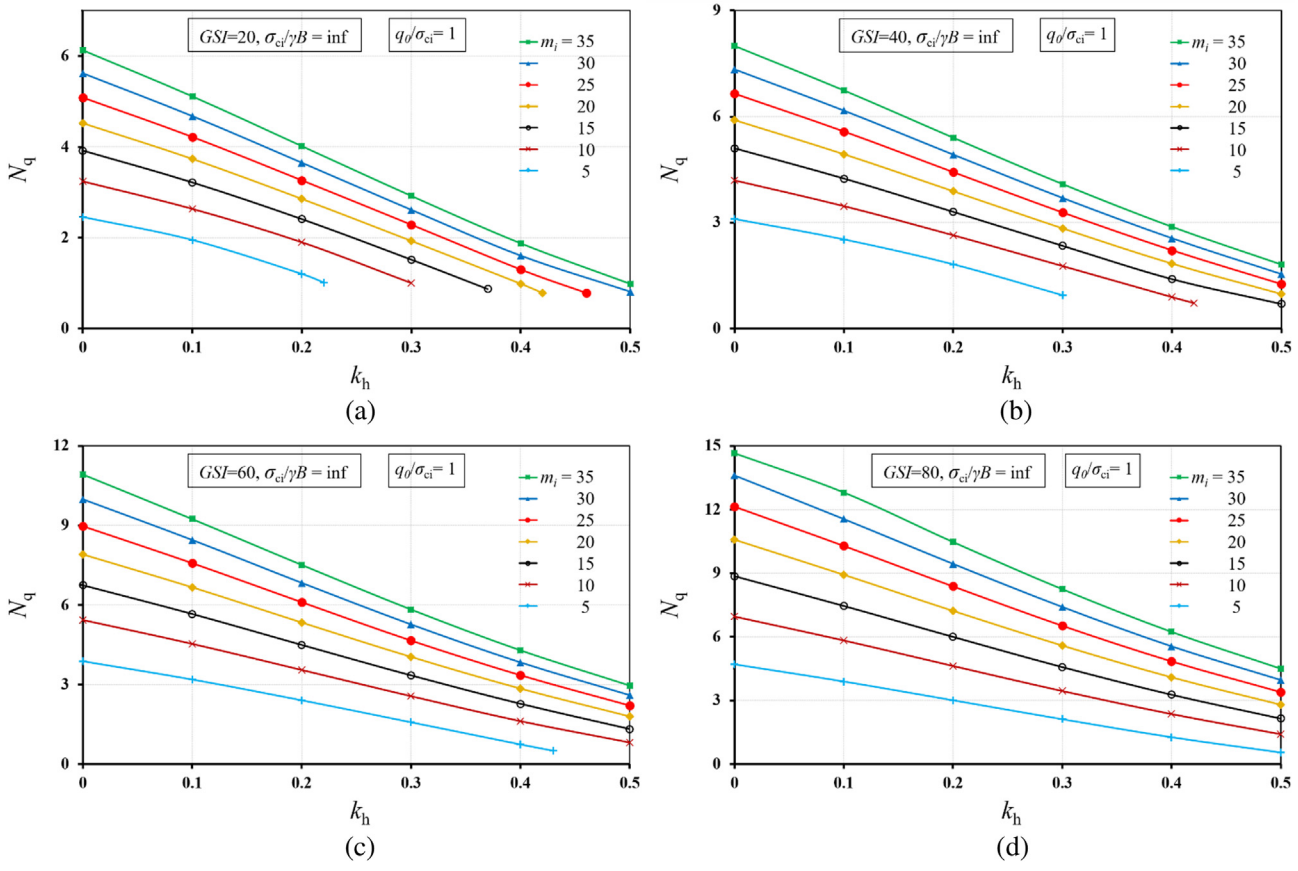

Fig. 13. Variation of N_q with k_h for $\sigma_{ci}/(\gamma B)$= inf and q_0/σ_{ci}= 1 for different m_i values with (a) *GSI* = 20, (b) *GSI* = 40, (c) *GSI* = 60, and (d) *GSI* = 80.

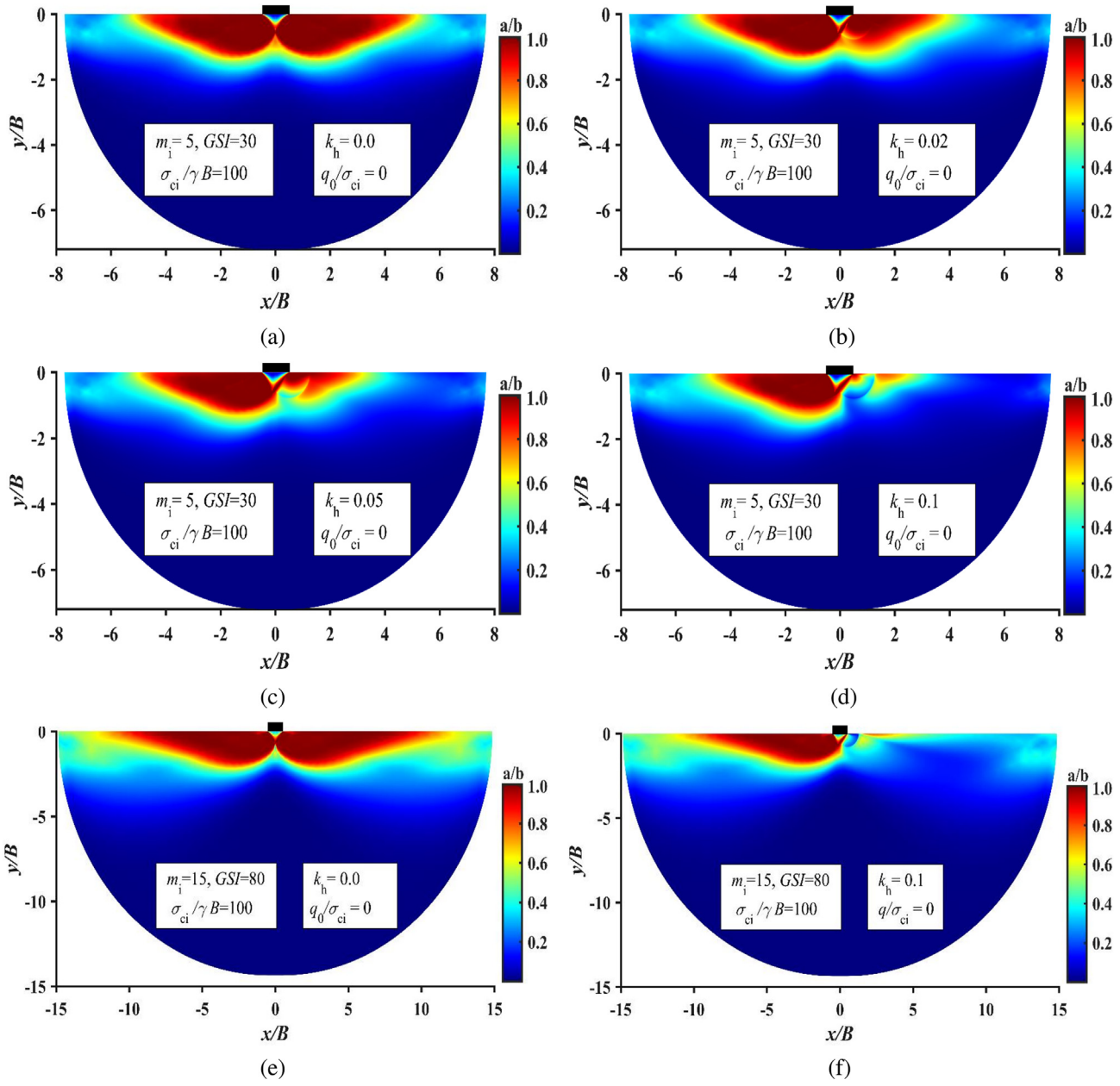

Fig. 14. The collapse mechanisms for $\sigma_{ci}/(\gamma B) = 100$ and $q_0/\sigma_{ci} = 0$ with (a) m_i=5, GSI =30 and k_h=0.0; (b) m_i=5, GSI =30 and k_h=0.02; (c) m_i=5, GSI =30 and k_h=0.05; (d) m_i=5, GSI =30 and k_h=0.1; (e) m_i=15, GSI =80 and k_h=0.0; and (f) m_i=15, GSI =80 and k_h=0.1.

symmetrical yielded zone, and the size of the yielded zone decreases continuously with an increase in surcharge pressure. Since the footing-rock interface is considered to be perfectly rough, in all the cases, a small non-plastic wedge is found to exist invariably below the footing base.

6. Conclusions

The LB FELA in conjunction with the PCP has been employed to compute in an accurate fashion the seismic bearing capacity factors for a strip footing lying on rock media. The yielding of rock media has been modelled by the GHB criterion. No approximation is needed to make any assumption either about the geometry of the failure mechanism or smoothing of the yield criterion. The effects of the equivalent inertial forces on the bearing capacity factors, induced due to an occurrence of earthquake, are accounted for by means of equivalent pseudo-static horizontal seismic forces with the usage of the earthquake acceleration coefficient (k_h). It has been observed that the bearing capacity factors N_σ and N_q decrease continuously with an increase in the magnitude of the earthquake acceleration coefficient (k_h). The magnitudes of N_σ and N_q increase continuously with an increase in the values of GSI and m_i. The failure patterns in the presence of the earthquake acceleration become always un-symmetrical. The size of the plastic zone increases with an increase in the values of GSI and m_i. The results provided in this study will be useful for designing strip footings on rock media in a seismically active zone.

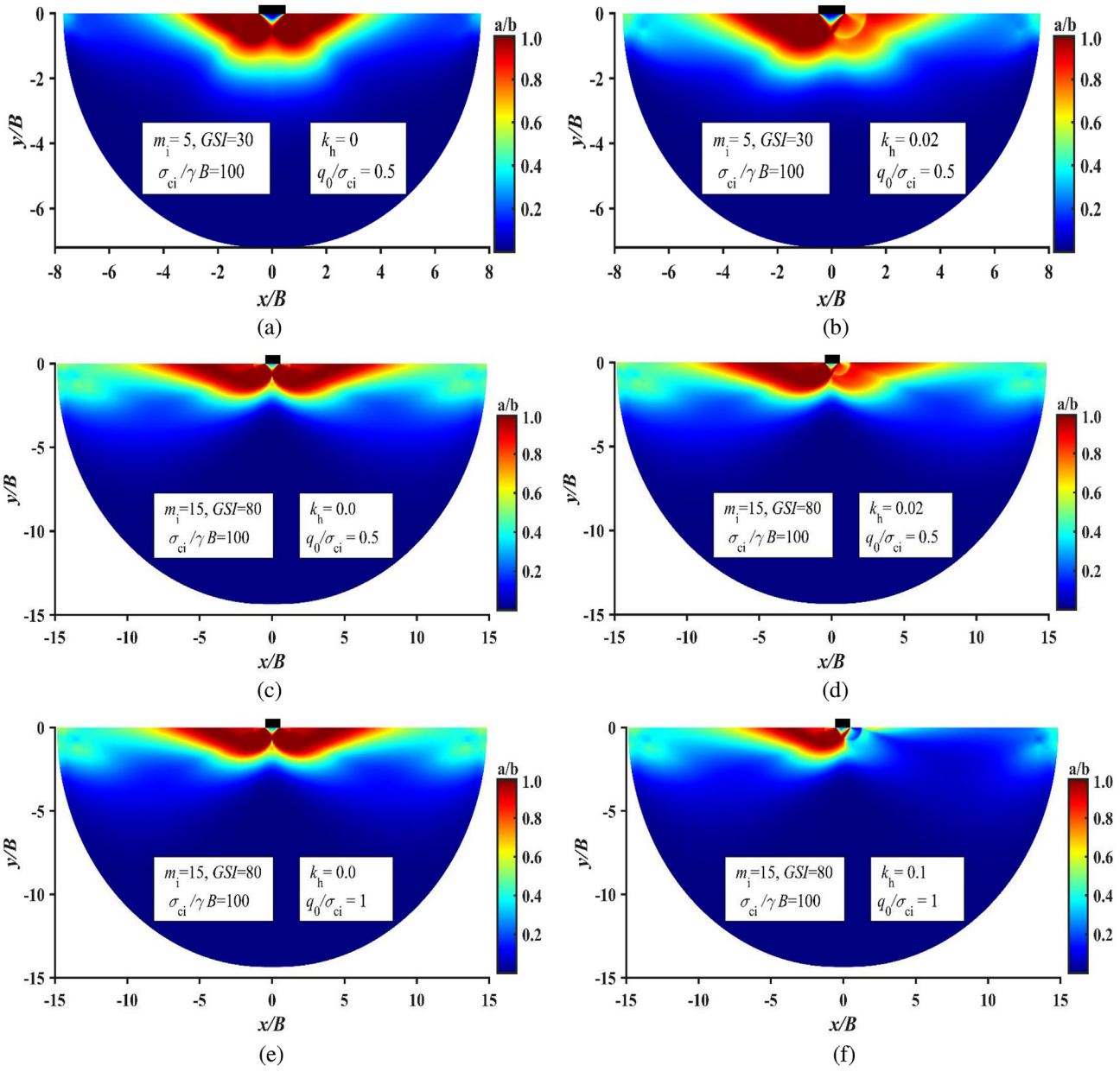

Fig. 15. The collapse mechanisms for $\sigma_{ci}/(\gamma B)$ = 100 with (a) m_i=5, GSI =30, q_0/σ_{ci}= 0.5 and k_h=0.0; (b) m_i=5, GSI =30, q_0/σ_{ci}= 0.5 and k_h=0.02; (c) m_i=15, GSI =80, q_0/σ_{ci}= 0.5 and k_h=0.0; (d) m_i=15, GSI =80, q_0/σ_{ci}= 0.5 and k_h=0.02; (e) m_i=15, GSI =80, q_0/σ_{ci}= 1 and k_h=0.0; and (f) m_i=15, GSI =80, q_0/σ_{ci}= 1 and k_h=0.1.

Declaration of competing interest

The authors declare that they have no known competing financial interests or personal relationships that could have appeared to influence the work reported in this paper.

List of symbols

B	Width of foundation
q_0	Surcharge pressure
γ	Unit weight of rock mass
k_h	Horizontal acceleration coefficient
g	Acceleration due to gravity
Q_u	Vertical collapse load
σ_1	Major principal stress
σ_3	Minor principal stress
σ_{ci}	Uniaxial compressive strength
m_b, m_i, s, α	Hoek-Brown material constants
GSI	Geological strength index
D	Disturbance factor
L_h	Horizontal extents of the circular domain
L_v	Vertical extents of the circular domain
σ_x	Normal stress on x-plane
σ_y	Normal stress on y-plane
τ_{xy}	Shear stress with respect in x-y plane
N_i	Shape function
σ_n	Normal stress
τ	Shear stress
$\boldsymbol{A}_{equi}$	Matrix containing the left hand side of all the equilibrium equations
$\boldsymbol{A}_{sd}$	Matrix containing the left hand side of all the discontinuity equations

$\boldsymbol{A}_{bc}$	Matrix containing the left hand side of all the boundary conditions
$\boldsymbol{A}_{eq}$	Matrix containing the coefficients of all the equality constraints
$\boldsymbol{A}_{cone}$	Matrix containing the coefficients of conic constraints
$\boldsymbol{b}_{equi}$	Vector containing the right hand side of all the equilibrium equations
$\boldsymbol{b}_{dis}$	Vector containing the right hand side of all the discontinuity equations
$\boldsymbol{b}_{bc}$	Vector containing the right hand side of all the boundary conditions
$\boldsymbol{b}_{eq}$	Vector containing the right hand side of the equality constraints
$\boldsymbol{b}_{cone}$	Right known vector of the conic constraints

Global unknown vector of stress variables

$\boldsymbol{\sigma}$	Global unknown vector of stress and slack variables
$\boldsymbol{x}_{cone}^{T}$	Global unknown vector of conic variables
t	An auxiliary variable
$\boldsymbol{c}$	Vector containing the objective function
NN	Number of nodes
q_u	Ultimate bearing pressure
N_σ	Bearing capacity factor due to unit weight
$N_{\sigma 0}$	Bearing capacity factor of weightless media
N_q	Bearing capacity factor due to surcharge
a, b	Parameters which defines the state of stress
$\wp^n$	n-dimensional power cone
$\Re^n$	n-dimensional real number

References

Andersen, E.D., Roos, C., Terlaky, T., 2003. On implementing a primal-dual interior-point method for conic quadratic optimization. Math. Program. 95 (2), 249–277.

Chakraborty, M., Kumar, J., 2015. Bearing capacity of circular footings over rock mass by using axisymmetric quasi lower bound finite element limit analysis. Comput. Geotech. 70, 138–149.

Chehade, H.A., Dias, D., Sadek, M., Jenck, O., Chehade, F.H., 2021. Pseudo-static analysis of reinforced earth retaining walls. Acta Geotech 16, 2275–2289.

Conte, E., Troncone, A., Vena, M., 2017. A method for the design of embedded cantilever retaining walls under static and seismic loading. Geotechnique 67 (12), 1081–1089.

Hoek, E., 1990. Estimating Mohr–Coulomb friction and cohesion values from the Hoek–Brown failure criterion. Int. J. Rock Mech. Min. Sci. Geomech. Abstr. 12 (3), 227–229.

Hoek, E., Brown, E.T., 1980. Underground Excavation in Rock. CRC Press.

Hoek, E., Brown, E.T., 2019. The Hoek-Brown failure criterion and GSI – 2018 edition. J. Rock Mech. Geotech. Eng. 11 (3), 445–463.

Hoek, E., Carranza-Torres, C., Corkum, B., 2002. Hoek-Brown failure criterion – 2002 edition. In: Proceedings of NARMS-Tac Conference, Toronto, pp. 267–273.

Hoek, E., Wood, D., Shah, S.A., 1992. Modified Hoek-Brown failure criterion for jointed rock masses. In: Proceedings of the International Symposium on Rock Characterization. International Society for Rock Mechanics, pp. 209–214.

Keshavarz, A., Fazeli, A., Sadeghi, S., 2016. Seismic bearing capacity of strip footings on rock masses using the Hoek–Brown failure criterion. J. Rock Mech. Geotech. Eng. 8 (2), 170–177.

Keshavarz, A., Kumar, J., 2021. Bearing capacity of ring foundations over rock media. J. Geotech. Geoenviron. Eng. 147 (6), 04021027.

Krabbenhoft, K., Lyamin, A.V., Sloan, S.W., 2008. Three dimensional Mohr-Column limit analysis using semidefinite programming. Commun. Numer. Methods Eng. 24 (11), 1107–1119.

Kulhawy, F.H., Carter, J.P., 1992. Settlement and bearing capacity of foundations on rock masses. In: Engineering in Rock Masses. Butterworth-Heinemann, pp. 231–245.

Kumar, J., 2001. Seismic passive earth pressure coefficients for sands. Can. Geotech. J. 38 (4), 876–881.

Kumar, J., Chakraborty, D., 2013. Seismic bearing capacity of foundations on cohesionless slopes. J. Geotech. Geoenviron. Eng. 139 (11), 1986–1993.

Kumar, J., Mohan Rao, V.B.K., 2002. Seismic bearing capacity factors for spread foundations. Geotechnique 52 (2), 79–88.

Kumar, J., Mohan Rao, V.B.K., 2003. Seismic bearing capacity of foundations on slopes. Geotechnique 53 (3), 347–361.

Kumar, J., Mohapatra, D., 2017. Lower-bound finite elements limit analysis for Hoek Brown materials using semidefinite programming. J. Eng. Mech. 143 (9), 04017077.

Kumar, J., Rahaman, O., 2020. Lower bound limit analysis using power cone programming for solving stability problems in rock mechanics for generalized Hoek–Brown criterion. Rock Mech. Rock Eng. 53 (7), 3237–3252.

Li, A.J., Lyamin, A.V., Merifield, R.S., 2009. Seismic rock slope stability charts based on limit analysis methods. Comput. Geotech. 36 (1–2), 135–148.

Li, A.J., Merifield, R.S., Lyamin, A.V., 2008. Stability charts for rock slopes based on the Hoek–Brown failure criterion. Int. J. Rock Mech. Min. Sci. 45 (5), 689–700.

Lysmer, J., 1970. Limit analysis of plane problems in soil mechanics. J. Soil Mech. Found Div. 96, 1311–1334.

Makrodimopoulos, A., Martin, C.M., 2006. Lower bound limit analysis of cohesive frictional materials using second-order cone programming. Int. J. Numer. Methods Eng. 66 (4), 604–634.

Merifield, R.S., Lyamin, A.V., Sloan, S.W., 2006. Limit analysis solutions for the bearing capacity of rock masses using the generalized Hoek-Brown yield criterion. Int. J. Rock Mech. Min. Sci. 43 (6), 920–937.

Pastor, J., Thai, T.H., Francescato, P., 2003. Interior point optimization and limit analysis: an application. Commun. Numer. Methods Eng. 19, 779–785.

Rahaman, O., Kumar, J., 2020. Stability analysis of twin horse-shoe shaped tunnels in rock mass. Tunn. Undergr. Space Technol. 98, 103354.

Saada, Z., Maghous, S., Garnier, D., 2008. Bearing capacity of shallow foundations on rocks obeying a modified Hoek-Brown failure criterion. Comput. Geotech. 35, 144–154.

Saada, Z., Maghous, S., Garnier, D., 2011. Seismic bearing capacity of shallow foundations near rock slopes using the generalized Hoek-Brown criterion. Int. J. Numer. Anal. Methods GeoMech. 35 (6), 724–748.

Saada, Z., Maghous, S., Garnier, D., 2013. Pseudo-static analysis of tunnel face stability using the generalized Hoek–Brown strength criterion. Int. J. Numer. Anal. Methods GeoMech. 37 (18), 3194–3212.

Sahoo, J.P., Kumar, J., 2012. Seismic stability of a long unsupported circular tunnel. Comput. Geotech. 44, 109–115.

Serrano, A., Olalla, C., 1994. Ultimate bearing capacity of rock masses. Int. J. Rock Mech. Min. Sci. Geomech. Abstr. 31 (2), 93–106.

Serrano, A., Olalla, C., 1996. Allowable bearing capacity of rock foundations using a nonlinear failure criterium. Int. J. Rock Mech. Min. Sci. Geomech. Abstr. 33 (4), 327–345.

Serrano, A., Olalla, C., Gonzalez, J., 2000. Ultimate bearing capacity of rock masses based on the modified Hoek–Brown criterion. Int. J. Rock Mech. Min. Sci. 37 (6), 1013–1018.

Sloan, S.W., 1988. Lower bound limit analysis using finite elements and linear programming. Int. J. Numer. Anal. Methods GeoMech. 12, 61–77.

Sloan, S.W., 2013. Geotechnical stability analysis. Geotechnique 63 (7), 531–571.

Suchowerska, A.M., Merifield, R.S., Carter, J.P., Clausen, J., 2012. Prediction of underground cavity roof collapse using the Hoek–Brown failure criterion. Comput. Geotech. 44, 93–103.

Tang, C., Toh, K., Phoon, K., 2014. Axisymmetric lower-bound limit analysis using finite elements and second order cone programming. J. Eng. Mech. 140 (2), 268–278.

Terzaghi, K., 1943. Theoretical Soil Mechanics. Wiley, New York, USA.

Terzaghi, K., 1950. Mechanism of landslides. In: Application of Geology to Engineering Practice. The Geological Society of America, pp. 83–123.

Ukritchon, B., Keawsawasvong, S., 2018. Three-dimensional lower bound finite element limit analysis of Hoek-Brown material using semidefinite programming. Comput. Geotech. 104, 248–270.

Ukritchon, B., Keawsawasvong, S., 2019. Stability of unlined square tunnels in Hoek-Brown rock masses based on lower bound analysis. Comput. Geotech. 105, 249–264.

Ulusay, R., 2014. The ISRM Suggested Methods for Rock Characterization, Testing and Monitoring: 2007-2014. Springer.

Yang, X.L., 2009. Seismic bearing capacity of a strip footing on rock slopes. Can. Geotech. J. 46, 943–954.

Yang, X.L., Yin, J.H., 2005. Upper bound solution for ultimate bearing capacity with a modified Hoek–Brown failure criterion. Int. J. Rock Mech. Min. Sci. 42, 550–560.

Yang, X.L., Yin, J.H., Li, L., 2003. Influence of a nonlinear failure criterion on the bearing capacity of a strip footing resting on rock mass using a lower bound approach. Can. Geotech. J. 40 (3), 702–707.

Dr. Jyant Kumar is currently working as a Professor in Department of Civil Engineering at Indian Institute of Science, Bengaluru, India. He received his BTech, MTech and PhD degrees in Civil Engineering from Regional Engineering College (NIT), Kurukshetra; Indian Institute of Technology, Kanpur; Indian Institute of Science, Bangalore in 1988, 1991 and 1994, respectively. He was affiliated as Scientist, Geotechnical Engineering Division, Central Road Research Institute, CSIR, New Delhi from 1993 to 1996; and Lecturer, Geotechnical Engineering, University of Technology, Lae, PNG from 1997 to 1999. His research interests include (1) lower and upper bound limit analysis with the usage of finite elements, meshless methods and conic programming; (2) slip line solutions in geomechanics; (3) in situ shear wave velocity profile of ground and pavements using multi-channel analysis of surface waves; and (4) the effect on saturation and stress cycles on dynamic properties of soils using resonant column and bender elements tests.